

**THE DESCENDING INFLUENCE OF BODY ORIENTATION ON
FORCE FEEDBACK IN THE DECEREBRATE CAT**

A Thesis
Presented to
The Academic Faculty

by

Christopher Tuthill

In Partial Fulfillment
of the Requirements for the Degree
Doctor of Philosophy in the
School of Biomedical Engineering

Georgia Institute of Technology/Emory University
May 2019

Copyright © Christopher Tuthill 2019

**THE DESCENDING INFLUENCE OF BODY ORIENTATION ON
FORCE FEEDBACK IN THE DECEREBRATE CAT**

Approved by:

Dr. T. Richard Nichols, Advisor
School of Biological Sciences
Department of Biomedical Engineering
Georgia Institute of Technology
Emory University

Dr. Boris Prilutsky
School of Biological Sciences
Georgia Institute of Technology

Dr. Young-Hui Chang
School of Biological Sciences
Department of Biomedical Engineering
Georgia Institute of Technology
Emory University

Dr. Randy Trumbower
Department of Physical Medicine and
Rehabilitation
Harvard Medical School

Dr. Charlie Kemp
Department of Biomedical Engineering
Georgia Institute of Technology
Emory University

Date Approved: January 6, 2019

TABLE OF CONTENTS

LIST OF FIGURES	vi
LIST OF ABBREVIATIONS	xiii
SUMMARY	xiv
CHAPTER 1 INTRODUCTION	1
1.1 Muscle Properties: Force Production	2
1.2 Muscle Properties: Proprioception	2
1.3 Muscle Properties: Reflexes	3
1.4 Ankle Extensor Anatomy	5
1.5 Task Specificity	6
1.6 Whole Limb Measurements	7
1.7 Body Orientation Signal	9
1.8 Summary	12
CHAPTER 2 INTERMUSCULAR FEEDBACK	13
2.1 Introduction	13
2.2 Methods	14
2.2.1 Decerebrate Cat Preparation	14
2.2.2 Labyrinthectomy	16
2.2.3 Muscle Dissection	17
2.2.4 Muscle Puller Apparatus	18
2.2.5 Head Tilt	20
2.2.6 Locomotion and Crossed Extensor Reflex	21

2.2.7 Data Processing	22
2.2.8 Analysis	25
2.2.9 Exclusions	26
2.3 Results	27
2.3.1 G-FHL (inhibitory feedback is modulated by head tilt)	28
2.3.2 FHL-G (modulation was not as consistent)	31
2.3.3 G/Sol	35
2.3.4 Control	38
2.4 Discussion	40
CHAPTER 3 ROBOTIC SYSTEM DEVELOPMENT	47
3.1 Introduction	47
3.2 Methods and Results	48
3.2.1 Equipment	48
3.2.2 System Integration	50
3.2.3 Spatial Sampling Pattern	52
3.2.4 Data Processing and Analysis	62
3.3 Discussion	71
CHAPTER 4 FELINE HINDLIMB STIFFNESS	76
4.1 Introduction	76
4.2 Methods	77
4.2.1 Surgical Preparation	77
4.2.2 EMG Electrode Implantation	78
4.2.3 Decerebration	81

4.2.4 Mechanical Support	83
4.2.5 Robotic System Integration	83
4.2.6 Robotic Data Collection	85
4.3 Results	87
4.4 Discussion	94
CHAPTER 5 DISCUSSION	98
REFERENCES	102

LIST OF FIGURES

- Figure 2.1 Muscle Puller System. Steel bone pins are inserted into the femur and tibia of each limb to be measured. The bone pins are rigidly clamped to a support frame over a treadmill belt. Muscles of interest are dissected so that they can move independently. The distal tendon of each muscle is affixed to a clamp which allows it to connect to linear motors with inline myograph force sensors. 18
- Figure 2.2 Force and Length Profiles. Each perturbation consists of a 2 mm stretch over 50 ms, a 100 ms hold phase, and a return to the resting position over 50 ms. The muscle designated as the recipient is first stretched alone and then simultaneously with the donor muscle providing intermuscular feedback. In this example, FHL is receiving inhibitory feedback from G. 20
- Figure 2.3 Raw Force and Interpolated Baseline. The blue trace is the raw force data from a recording during XER. At this timescale the individual stretch perturbations appear as spikes on in the raw force record. The green curve was created by replacing the stretch responses with a linear interpolation. This approximates the underlying XER curve. 23
- Figure 2.4 Force response curves are divided into different epochs. The blue shading indicates the phase prior to the stretch and is the background force against which the force responses are compared. The red area is the first 10ms after the stretch is initiated; any separation between states in this epoch indicates mechanical coupling between muscles as no reflex activity is fast enough to be present at this period. The green, purple, and orange areas represent the early, middle, and late epochs, respectively. These epochs cover the entire 100 ms hold phase. 25

Figure 2.5 G inhibits FHL during locomotion. In the level condition, there is moderate inhibition from G onto FHL. This inhibition increases downhill condition (head tilted up 20°). In the uphill condition (head tilted down 20°) the inhibition is diminished to the point where there is no statistically significant distinction between the curves. 28

Figure 2.6 Comparison of intermuscular inhibition from G to FHL under XER. The square markers indicate FHL's autogenic response which were very similar between head positions. The open circles show FHL's response force when stretched with G. All head positions show that G provides inhibitory feedback to FHL, but the magnitude of inhibition increases with increasing head angle. 30

Figure 2.7 Feedback from FHL to G during locomotion. The square markers indicate autogenic G responses and the open circles represent the G responses when stretched with FHL. The feedback from FHL to G during locomotion shows increasing inhibition with increasing head pitch. This mirrors the feedback in the opposite direction showing that G and FHL are mutually inhibitory and that their inhibition retains its symmetry over the range of simulated ramp angles. 32

Figure 2.8 Inhibitory feedback from FHL to G during XER. The closed markers indicate autogenic G responses and the open markers are G responses when stretched with FHL. The inhibition from FHL to G during XER also showed a trend of reduced inhibition with increased simulated slope angle. G did not always respond to XER, even when its viability was confirmed by the feedback provided in the opposite direction to FHL. 34

Figure 2.9 Sol provides excitatory feedback to G during locomotion. The closed square markers indicate the autogenic response of G and the open circles represent the G responses when stretched with Sol. The range of G background forces is diminished in the non-level conditions, but the excitatory feedback appears to be slightly greater with head tilt. 36

Figure 2.10 Excitatory feedback from Sol to G does not appear to vary with head tilt during XER. The magnitude of excitation appears to be smaller than what was observed under locomotion. 37

Figure 2.11 Control experiments with no labyrinthectomy show that reflex responses are invariant with head tilt. In both plots the solid square markers show the autogenic responses of the recipient and the open circles indicate the responses when stretched with the donor muscle. Plot A shows that all conditions produce the same level of inhibition from G to FHL and plot B shows the same for excitatory feedback from Sol to G. 39

Figure 2.12 Theoretical extrapolation accounting for apparent reversal of head tilt relationship. The autogenic curves of FHL appear to have the opposite trend in this study as compared to what was reported by Ross (2006). The range of background forces was different between the two studies and this graph demonstrates an example of curves that could account for both findings. If the curves intersect near the background force indicated by the dashed line, the progression between head positions appears to be opposite on either side of this intersection. 42

Figure 3.1 Schematic of the robotic stiffness measurement platform. The robot controllers use a CAN bus to sample data from the force/torque sensors (not pictured).

Instructions for each perturbation are sent over ethernet and the results from each perturbation are sent back to the PC after each perturbation. An analog signal is sent from one of robot controllers to the Vicon system which allows for the synchronization of the robot and force data with the EMG and kinematic data. 51

Figure 3.2 Diagram of the Clockface and Rotate pattern. This technique yields a sampling pattern of intersecting circles. While this grid pattern is intuitive due to its similarity to the latitude/longitude system used in cartography, the distribution is biased towards the poles of the z-axis. While an evenly distributed sampling pattern is not necessary for the accurate calculation of limb stiffness, oversampling at an arbitrary position results in unnecessarily lengthy collection times. 54

Figure 3.3 Example of 50 perturbation directions approximately evenly distributed. The golden spiral method is used to generate these points as it can be used with arbitrarily selected totals. Perfectly distributed points can only be achieved with specific totals that correspond to the vertices of Platonic solids. Evenly distributed perturbations are preferred for initial measurements as a poorly distributed set could introduce bias to the calculated stiffness ellipsoid. 56

Figure 3.4 Using a single perturbation direction, whole limb force responses were collected during XER and the average force magnitudes were plotted. Student's t-test was used to determine that the downhill condition showed a statistically significant reduction in scalar force response in the shaded region. This confirmed that head tilt does produce whole limb biomechanical alterations and that these changes could be measured with our equipment. 58

Figure 3.5 The first phase of the dynamic major axis search uses even distributed perturbation directions (A) to get an initial set of force responses. A stiffness ellipsoid is calculated from these perturbations and a new set of perturbations (B) is generated clustered around the major axis of the ellipsoid. The stiffness ellipsoid is recalculated to include the new data and a third set of perturbations (C) is generated in the plane of the major axis which improves the sample density at the minor axes. The overall set of perturbation directions (D) samples densely in the regions where the responses change the most rapidly and sparsely where the curvature is less pronounced. 61

Figure 3.6 Using the clockface and rotate sampling pattern, force magnitudes can be mapped onto a 2D projection. The color scale indicates normalized scalar magnitude at the coordinates indicated by azimuth on the horizontal axis and elevation on the vertical. While this allows the easy visualization of the measured space, force directionality is not preserved. 63

Figure 3.7 The stiffness matrix is calculated at sample over the time course and each element is plotted individually. The stiffness matrix fluctuates significantly at the start of the perturbation (0-100 ms) but settles near the end of the movement and through the hold phase. The centroid can also be plotted in this fashion using a y-axis with units of force. 66

Figure 3.8 The stiffness ellipsoid is visualized by multiplying the stiffness matrix k by a unit sphere. Scaling by the length of the perturbations gives a force ellipsoid which corresponds to a geometric fit of the measured forces. The color scale indicates

vertical component of stiffness and is included for the purpose of improving the visualization of the ellipsoid shape. 67

Figure 3.9 By projecting the cloud of force responses onto the anatomical planes allows for easier visualization in 2D. This also facilitates comparisons with results from studies that were performed in 2D. 68

Figure 3.10 Raw EMG contained substantial movement artifacts and mains noise. The top row of plots taken from the largest response of aBF and the bottom row is the minimum response from the same trial. The EMG is filtered with both a bandpass filter and a 60 Hz notch filter allowing muscle activity to be isolated. In these examples the bandpass filter was set to 20-125 Hz to better illustrate the filter performance at the cutoff frequencies. 69

Figure 3.11 EMG can be plotted against perturbation direction with marker size indicating integrated RMS EMG magnitude. The blue circles represent increased EMG activity while the red diamonds denote a reduction in EMG activity as compared to baseline. 71

Figure 4.1 Projected passive ellipsoids show reduced overall stiffness in the head up condition. The level and head down ellipsoids have very similar sizes but are oriented slightly differently. While we expected a progressive change between head angles this shows that more complex strategies may be responsible for the alterations needed for sloped task. 89

Figure 4.2 Average force responses during XER along a single perturbation axis show reduced force in the downslope case as compared to level and uphill. This matches

the trend found with 3D measurements in the passive condition which suggests that the change in apparent force is due to reduced limb stiffness. 90

Figure 4.3 Control experiments were performed under isoflurane anesthesia. As expected, all 3 head tilt conditions resulted in nearly identical stiffness ellipsoids. In these trials the limbs were entirely flaccid and the stiffness measured is representative of the purely structural components of the leg. While the force magnitude is significantly lower than those measured in active conditions, the eccentricity and orientation of the ellipsoid is very similar. 92

LIST OF ABBREVIATIONS

CNS	Central Nervous System
DOF	Degrees of Freedom
DOI	2,5-Dimethoxy-4-iodoamphetamine
ETCO ₂	End-Tidal Carbon Dioxide
FHL	Flexor Hallucis Longus Muscle
G	Gastrocnemius Muscle
GTO	Golgi Tendon Organ
HR	Heart Rate
LG	Lateral Gastrocnemius Muscle
MG	Medial Gastrocnemius Muscle
MTP	Metatarsophalangeal Joint
PI	Plantaris Muscle
RR	Respiratory Rate
Sol	Soleus Muscle
SpO ₂	Peripheral Oxygen Saturation
XER	Crossed-Extensor Reflex

SUMMARY

Humans and animals interact with a variety of terrain with sloped surfaces being one of the most fundamental. As the biomechanical requirements for walking on sloped surfaces changes with the angle of incline and direction of travel, the nervous system must have an efficient means to tune the motor output to meet these variable requirements. We hypothesized that this tuning is achieved by altering the gains of intermuscular force dependent spinal reflexes. We tested this hypothesis using the decerebrate cat model with vestibular labyrinthectomy which allowed for the simulation of sloped support surfaces by manipulating the angle of the neck. We measured the changes in intermuscular force feedback by stretching individual ankle extensor muscles in various combinations during background motor patterns such as stepping and crossed extensor reflex. We also measured the changes in endpoint stiffness of the cat hindlimb using a newly developed robotic system.

We found that certain pathways of inhibitory force feedback, such as between gastrocnemius and flexor hallucis longus, were enhanced in the downhill cases and somewhat diminished in the uphill conditions. These findings corresponded to a measured decrease in hindlimb stiffness during downhill conditions; however, the uphill cases did not exhibit any trend of altered stiffness. Both the increased inhibition and decreased stiffness for downhill matched our expectations as a more compliant limb is needed to provide braking action rather than producing propulsive force. The greater variability in our uphill experiments possibly indicates that multiple successful strategies exist under these conditions or that the patterns are very similar to level conditions and the differences are too subtle to resolve with our methods.

CHAPTER 1

INTRODUCTION

It is well known that in order for a motor task to be successful it must match the demands of the environment. Even the seemingly simple task of standing in place is only possible if the center of mass is kept over the base of support. In order to achieve this minor feat, the body must coordinate the activity of numerous muscles throughout the body on a continuous basis. The reason this complex task seems simple is that we are not consciously aware of the prodigious amount of neural processing that is performed in the spinal cord (Pierrot-Deseilligny and Burke 2012). In addition to producing these basic motor outputs the spinal cord must be able to alter these patterns to respond to different environments or unexpected perturbations.

Even subtle environmental changes such as the difference between standing on a sloped and level surface require the spinal cord to produce distinctly different motor patterns (Gottschall and Nichols 2011). In order to shift between these tasks numerous systems must coordinate. Information about the environment must be detected and transmitted to the spinal circuitry responsible for generating the motor patterns which then must adopt a new more appropriate strategy. Just like the basic task of standing on a level support surface all of these complex neural interactions occur continuously and sible, it should be possible to adapt these methods for use with trained casor??humans. this sloped surface challenge it is a frequently used model for understanding task specificity. In this study we aimed to uncover the neural basis of this adaptation and to document the resulting biomechanical changes that they cause.

1.1 Muscle Properties: Force Production

One of the fundamental properties of muscle is its force production ability. Force is generated by extrafusal muscle fibers which typically make up the majority of a muscle's mass. The contraction of these muscle fibers is initiated by the release of acetylcholine from alpha motor neurons. The alpha motor neuron and the muscle fibers that it innervates comprise a motor unit and is the finest muscle element that the central nervous system (CNS) can control. The CNS can modulate the amount of force produced by the muscle both by altering the number of motor units that are recruited and by increasing the firing rate of individual motor units. In this study we measured the patterns of force production to gain insight into how the CNS adopts new strategies based on environmental cues.

1.2 Muscle Properties: Proprioception

In addition to the extrafusal fibers, muscles contain sensory cells that detect the mechanical state of the muscle. Collectively, these sensors provide the CNS with the information needed to know the relative positions of all body segments as well as the amount of force being produced or applied to the body; this gives rise to the sensation known as proprioception. This is mostly achieved through the use of muscle spindle receptors which detect the length of each muscle and Golgi tendon organs (GTOs) which are sensitive to force.

Muscle spindles contain contractile elements known as intrafusal muscle fibers. The intrafusal fibers are innervated by gamma motor neurons. The activation of the

intrafusal fibers does not significantly contribute to the muscle's force production, but rather modulates the sensitivity of the sensory afferents. Muscle spindles contain type Ia sensory afferents which fire when the muscle length increases and type II fibers which fire continually based on the muscle's position. The muscle spindles are distributed throughout the muscle belly embedded in parallel with the extrafusal fibers which is necessary to accurately sense the position and lengthening velocity of the muscle.

Golgi tendon organs, as the name implies, are located in the musculotendinous junction. In anatomical contrast to the muscle spindles, the GTOs are in series with the muscle belly which is necessary for the accurate detection of force. It was previously believed that GTOs were only activated at very high levels of force and thus only served a protective function; however, this was subsequently disproven (Houk and Henneman 1967). The GTOs are innervated by type Ib sensory afferents whose firing rate is proportional to the muscle force over the entire physiological range.

These proprioceptors are not only activated by mechanical changes caused by contraction of the extrafusal fibers but by external perturbations as well. In this study we made extensive use of this by applying specific mechanical perturbations to muscles thereby activating the proprioceptors. The purpose of this study was to gain an understanding of how the CNS responds to this sensory information (Matthews 1972).

1.3 Muscle Properties: Reflexes

In addition to providing the sense of proprioception, the information provided by the muscle spindles and GTOs is also used in the spinal cord in the form of reflex circuits. A spinal reflex arc originates with sensory information in the peripheral nervous

system which is processed entirely in the spinal cord and results in a motor output. It is these reflex pathways that allow for a substantial portion of motor control to be performed without conscious intervention.

A significant portion of the reflex pathways from the musculature are length dependent. While these reflexes can be structurally as simple as a monosynaptic circuit the reflexes can be very complex due to the complicated nature of muscle spindle firing patterns. In spite of this, the length dependent reflexes have been extensively studied and are well documented (Nichols et al. 1999). The majority of these reflexes are excitatory and autogenic, the motor target is the same muscle from which the sensory signal originated (Eccles et al. 1957). Considering length as a control variable this creates a negative feedback system by which increases in muscle length cause the same muscle to contract and thus shorten. This has the functional effect of regulating muscular stiffness over a wide range of forces (Nichols and Houk 1976). This regulation in biarticular muscles results in enhanced interjoint coupling (Nichols et al. 1999). Allogenic length dependent reflexes also exist but are limited to muscles of similar mechanical action (Nichols 1999).

While the functional properties of length dependent reflexes have been well documented, the role of force dependent reflexes is not fully known. In contrast to the autogenic length reflexes, feedback from Golgi tendon organs is largely intermuscular and have limited connections to the originating muscle (Eccles et al. 1957; Nichols 1989). Additionally, the GTOs of a single muscle can contribute to the reflex response of multiple target muscles which results in a network of feedback between muscles. Force feedback does not contribute significantly to the regulation of individual muscle stiffness

(Bonasera and Nichols 1994; Nichols et al. 1999), however due to the distributed nature of these pathways it is likely that they contribute to the control of whole limb stiffness and interjoint coordination. Since the mechanical alterations required to shift between differently sloped surfaces likely requires alterations to multiple joints we hypothesized that network of intermuscular force feedback is harnessed to meet the demands of these tasks.

1.4 Ankle Extensor Anatomy

The ankle extensors of the cat were of particular interest to this study due to their anatomy and historical precedent. The muscles studied individually (gastrocnemius (G), soleus (Sol), flexor hallucis longus (FHL), and plantaris (Pl)) all have a narrow distal tendon which allows for the attachment of various external apparatuses necessary for experiments. Furthermore, all of these muscles are easy to access due to their location on the dorsal-posterior aspect of the shank and their close proximity to each other allows all of them to be accessed by a single dissection procedure. Finally, despite the anatomical similarities, the individual muscles have distinct functionality which can contribute to our understanding of how the exchange of proprioceptive information affects limb movements.

The G consists of two heads, the medial gastrocnemius (MG) and the lateral gastrocnemius (LG.) The lateral head originates from the lateral condyle of the femur and the medial head originates from the medial condyle. The heads are innervated separately and due to originating on opposite sides of the femur they have slightly different mechanical action; however, since they cannot be separated without risking damage we

treated the group as a single muscle for part of this study. The heads combine to form the calcaneal tendon, sometimes referred to as the Achilles tendon, which inserts into the posterior side of the calcaneus. The primary function of G is plantarflexion and also contributes to ankle abduction and knee flexion (Crouch 1969).

Sol is uniarticular and originates from the lateral side of the fibula and inserts on the calcaneus as part of the calcaneal tendon. In the domestic cat the Sol is composed entirely of slow twitch muscle fibers (McPhedran et al. 1965). This feature is not common among mammals and is not shared with humans. The action of Sol is almost entirely plantarflexion. Due to their common action, location, and distal tendon MG, LG, and Sol are often considered together as a group known as the triceps surae.

FHL originates from the fibula and while its muscle belly is entirely in the shank its distal tendon spans the length of the foot and inserts onto the ventral aspect of the toes. As a result, it serves to flex all the toe joints as well as contributes to ankle plantarflexion. Since felines normally walk and stand digitigrade the control of the toes and the metatarsophalangeal (MTP) joints is much more important than animals that tend to be plantigrade such as humans (Goslow et al. 1973).

1.5 Task Specificity

There are fundamental energetic differences required for movement on sloped surfaces. Uphill movement requires additional work to oppose the force of gravity. Conversely, gravitational potential energy provides some of the propulsive force for downhill movements. There are additional differences in the biomechanical requirements for sloped walking as animals must also maintain posture and control their velocity.

Walking upslope requires a stiff limb in order to transmit propulsive forces to the ground whereas downslope walking requires some muscles to be stretched eccentrically to provide braking force (Gregor et al. 2006; Maas et al. 2010). The cat also adopts an increasingly crouched posture with increased incline (Carlson-Kuhta et al. 1998). We expect that these alterations in muscle activity and posture should result in measurable mechanical changes to the hindlimb of the decerebrate cat.

1.6 Whole Limb Measurements

Despite the multitude of individual muscles and reflex pathways that contribute to the mechanics of a limb the net force and positioning of the limb are the ultimate factors which determine the outcomes of interactions with external bodies. Of particular importance are the mechanical properties at the distal end of the limb because hands, feet, and paws are where contact with external objects most commonly occurs in legged animals. The most common method of measuring the mechanical properties at the limb endpoint is to apply an external displacement perturbation and measure the resulting force response.

Prior studies with the decerebrate cat have used a moving platform to provide positional perturbations. These platforms typically take the form of a 2 degree of freedom (DOF) robots consisting of 1 rotational joint and 1 prismatic joint which allow for radial perturbations at arbitrary angles around a fixed origin. (Macpherson et al. 1986; Honeycutt and Nichols 2010). This method mimics the conditions of a slip event when the support surface suddenly moves with respect to the limb, however since the paws are adhered to sensors the normal cutaneous sensation associated with a genuine slip is not

present. This technique allows for the calculation of an endpoint stiffness ellipse. While this helps to understand postural corrections to slipping conditions, the calculated stiffness ellipse is restricted to the horizontal plane because the perturbations are only performed in this plane. This essentially provides a cross sectional perspective of the whole limb mechanics in 3 dimensional space.

Since the largest muscles of the leg contribute to flexion and extension and are used for forward propulsion and gravity resistance the largest component of the net force produced by the leg is perpendicular to the horizontal plane. As a result, any modulation of limb stiffness orthogonal to the horizontal plane are essentially invisible to the moving platform apparatuses.

Planar perturbations have also been used in the sagittal plane on the decerebrate cat forelimb (Martin 2013). This was achieved using the robotic arm system developed in this study. While measuring in the sagittal plane would capture changes occurring along the limb axis it precludes observation of changes that might occur due to abduction or adduction. This is possibly even more critical in the forelimb than the hindlimb as the forelimb are used for reaching and manipulation tasks in addition to locomotion and maintaining posture.

Regardless of which plane is chosen to apply perturbations a 2 dimensional system can never take into account the in-plane force contributions that would be caused by off-plane perturbations. Due to this, the development of a system to measure endpoint stiffness in 3 dimensions was needed to fully understand how the limb mechanics are altered by the body orientation signal.

1.7 Body Orientation Signal

There are three primary sensory systems that contribute to the sensation of body orientation: visual, vestibular, and proprioceptive (Kandel et al. 2013). By integrating different sources of information, the nervous system can normally construct a robust model of how the body is oriented with respect to the external environment. The visual system uses a number of cues to establish the relationship between the body and the objects in the visual field. Of chief importance are lines that are known or assumed to be horizontal or vertical such as the horizon or tall buildings (Magnus and de Kleijn 1912).

The vestibular system can detect linear acceleration using the utricle and saccule organs of the inner ear. The inner ear is filled with a viscous fluid called endolymph which is laden with small otolith particles. Hair cells within the utricle and saccule have mechanoreceptors which respond to the movement of endolymph and otoliths by depolarizing or hyperpolarizing the cells. Even when the body is stationary these organs are continuously responding to the acceleration caused by earth's gravitational field (Kandel et al. 2013). Information about the direction of gravity is important for correctly determining the slope of a support surface as well as for landing tasks such as the righting reflex.

As previously discussed the proprioceptive system consists of length and force sensors that are distributed throughout the body's musculature. The direction and magnitude of acceleration due to earth's gravity can be calculated by the proprioceptive system based on the amount of force required to resist it. Knowledge of the body's position relative to itself is critical for the successful application of the body orientation

signal since positioning of the limbs is typically what determines an animal's base of support. While the proprioceptors in all muscles contribute to the body orientation signal, the stretch receptors in the neck are critically important because they establish the positional relationship between the head and the rest of the body. Without an accurate measure of the neck angle the information provided by the visual and vestibular systems cannot be put into the frame of reference needed to provide a useful body orientation signal (Boyle and Pompeiano 1981; Ezure and Wilson 1984).

Under normal conditions these three systems complement each other to generate a unified representation of the body orientation. However, due to unusual conditions or sensory disorder the information from these different sources can come into conflict which requires the nervous system to compensate. A very common example of this is the motion sickness experienced on a moving vehicle. When the vehicle accelerates either due to intentional propulsion or inconsistent travel conditions the vestibular system senses the acceleration, but objects in the field of view that are contained in the vehicle appear stationary since they are moving at an identical rate to the eyes. A common strategy to mitigate this is to fixate one's gaze on an object external to the vehicle. This method "corrects" the disagreement by forcing the visual system to see the motion that is felt by the vestibular organs.

When conflicting information cannot be corrected, the nervous system must adapt. For example, in the immersive visual environment of virtual reality the images in the visual field are entirely artificial; however, subjects can often get the illusion of movement despite remaining stationary. This demonstrates that while the redundant sources of information help to create an accurate body orientation signal, they are not

individually necessary. Furthermore, those with vision or vestibular loss are able to use their remaining sensory systems to maintain a correct sense of body orientation (Putkonen et al. 1977).

In the decerebrate cat, which by definition does not have a visual cortex, it has been demonstrated that alterations of the neck pitch cause muscle activation patterns that match those of intact cats on a sloped surface (Gottschall and Nichols 2007). However, with an intact vestibular system driving the body orientation signal, the activation patterns are rapidly corrected and return to those which are normal for level surfaces. Additionally, Gottschall and Nichols (2007) found that by surgically disrupting the vestibular system, leaving proprioceptive input as the sole source of body orientation information, the altered motor patterns were still controlled by neck pitch and would remain this way until the neck pitch was changed again. These results are somewhat corroborated by Ezure and Wilson (1984) who also found neck and vestibular reflexes to be in opposition of each other in the decerebrate cat.

Due to this oppositional nature between the neck proprioceptors and the vestibular system, the pitch of the neck and grade of the support surface are negatively correlated. In intact animals this relationship can be observed in the behavioral tendency to maintain a head position that is level with gravity despite the posture that the rest of the body may take (Green 1998). Functionally, this behavior might be useful to standardize the inputs from the visual and vestibular systems, but in the decerebrate cat it can be used experimentally to produce task specific motor output

1.8 Summary

While there has been extensive research focusing on the properties of proprioceptive reflexes as well as studies that establish the different biomechanical requirements of sloped walking and standing tasks the contributions of the former to the latter have not been established. In this study we used the decerebrate cat to identify the changes in reflex patterns that exist between different slope conditions. We hypothesized that force dependent reflexes would be the target of modulation and that the magnitude of inhibition would increase oppositely of slope angle.

Additionally, we sought to measure the changes in limb stiffness under different sloped conditions. In order to achieve this, we needed to develop a new robotic system that would allow for measurements to be taken in 3 dimensional space. While the new system was developed for the decerebrate cat, it is highly configurable and can potentially be used in numerous other applications.

Both aspects of this study have the potential to translate to clinical applications. Understanding the mechanism that the spinal cord uses to produce task specific output could inform future treatments in the case of spinal cord injury. The robotic system could be used to measure limb stiffness either as a diagnostic test or to track the progression and recovery of an injury. A highly accurate measure of a patient's injury could lead to therapies that are customized to their needs. Furthermore, the robotic system has the capacity to be programmed to provide other functions such as measuring the stiffness of a single joint or even making stiffness measurements during movement. It would thus be possible to provide an entire suite of clinically relevant tasks in a single apparatus.

CHAPTER 2

INTERMUSCULAR FEEDBACK

2.1 Introduction

Sloped surfaces are extremely common in the natural environment and the ability to operate effectively on an incline is nearly as fundamental as on a level surface. When ascending a sloped surface more propulsive force is needed to resist gravity and conversely, when descending less force is needed due to the assistance of gravity. We know from previous studies (Nichols 2018) that intermuscular feedback is modulated to achieve different tasks. It is expected that the modulation of intermuscular feedback is a likely control mechanism for successful motor tasks on surfaces of varied inclination.

Length based sensory feedback predominantly affects the muscle in which the spindle receptors (Eccles et al. 1957) are located which precludes its use for widespread coordination. Force feedback originating from Golgi tendon organs has a more broadly distributed effect. The network of force dependent intermuscular feedback can be used to coordinate activity between joints which would be necessary for the adaptations necessary to switch between surfaces of different slopes.

It has been shown (Gottschall and Nichols 2007) that in the decerebrate cat tilting the head during locomotion results in electromyographical (EMG) patterns that match those found during ramp walking in intact cats. Since the decerebrate cat has a highly restricted set of sensory inputs to provide the spinal cord with environmental context we were able to manipulate the body orientation signal to indicate sloped conditions while keeping the hindlimbs stationary. This allowed us to make direct force recordings and

stretch perturbations on individual muscles. Using this technique, we were able to identify some of the changes to force feedback between different head tilt angles.

We hypothesized that compared to level, the downslope condition will exhibit increased intermuscular inhibition and that the inhibition will conversely be decreased for upslope. This hypothesis is in concert with the differing energetic requirements of sloped locomotion and for standing could represent a strategy for repositioning the center of mass to increase balance stability.

2.2 Methods

2.2.1 Decerebrate Cat Preparation

The decerebrate cat has historically been the gold standard for studying spinal reflexes. The muscular anatomy of the domestic cat has a very strong homology with humans even in spite of the obvious difference such as being digitigrade and quadrupedal. Additionally, cats are reasonably trainable which allows for comparison between decerebrate and intact animals. By using a decerebrate preparation we were able to remove anesthesia after performing highly invasive surgical procedures that would be impossible to achieve in a non-decerebrate cat. All procedures used in this study were approved by the Institutional Animal Care and Use committees at Georgia Institute of Technology and Emory University.

30 cats ranging from 3.5-6 kg were deeply anesthetized with isoflurane. Isoflurane was selected as it has a rapid onset of action as well as a rapid dispersal. A tracheotomy was performed to ensure a consistent airway was maintained throughout the experiment. After initial induction, an isoflurane concentration of 2-4% was administered. The isoflurane was mixed with a 95% O₂, 5% CO₂ blend which ensured

maximal oxygenation and respiratory drive. The concentration varied between preparation and we attempted to use the lowest levels as possible while still maintaining unconsciousness. In all but 1 preparation the cat was able to breathe without artificial ventilation while under anesthesia. Anesthesia was confirmed by monitoring withdraw responses and muscular tone. Vital signs (HR, RR, SpO₂, ETCO₂, and temperature) were monitored throughout the experiment using a SurgiVet Advisor vital signs monitor.

A loosely tied loop of suture was placed around each carotid artery during the initial surgery giving us the option to reduce the blood supply during the subsequent decerebration process. While preventing blood loss is important, keeping the surgical field clear is important as visualizing brainstem structures is critical to a successful decerebration. An external jugular vein was cannulated to provide intravenous access for the administration of fluids (either lactated ringers or normal saline) and, at the end of the experiment, euthanasia (1mL Euthasol or 20 mL saturated KCl.)

After the cat was rigidly fixed in a stereotaxic frame, a craniotomy was performed using a trephine and rongeurs. Bone wax was used to seal the exposed edges of the skull to prevent bleeding or air emboli. The cerebral cortices were removed with a spatula exposing the brainstem. The brainstem was transected and all brain matter rostral to the transection was removed via suction. In 13 experiments, a premammillary transection where the brainstem was cut at an angle immediately rostral to both the superior colliculus and the mammillary bodies was used to produce a state in which spontaneous locomotion can occur. A majority of experiments used a precollicular transection where a single vertical cut was made rostral to the colliculi and is used to produce a stable state

that is susceptible to electrical stimulation without the interference of spontaneous motor activity.

After the decerebration was completed, the skull was packed with hemostatic materials such as Gelfoam, QuikClot, and cotton balls. Isoflurane anesthesia was gradually reduced over 20 – 30 minutes. Removing the anesthesia rapidly had the potential to cause significant bleeding due to the sudden increase in blood pressure. Although muscle tone begins to return immediately, we found that spinal reflexes often did not recover as quickly which required an additional 30 minute recovery period after isoflurane had been removed.

Some cats experienced respiratory arrest during or shortly after the decerebration procedure. This is usually attributed to damage to the respiratory drive centers due to excessive movement of the brainstem during the decerebration. In these cases, external ventilation was provided. We did not find that this had any negative effect on either type of preparation. However, respiratory failure outside of this initial phase of the experiment was usually indicative of a declining preparation.

2.2.2 Labyrinthectomy

In a prior study it was found that the effect of head tilt was transient if the vestibular system was left intact (Gottschall and Nichols 2007). In order to prevent the vestibular system from compensating for the effects of neck angle, the vestibular labyrinths were surgically disrupted which allowing the changes due to neck angle to become static. Typically, the labyrinthectomy was performed concurrently with the initial surgery and a ventral approach was taken to visualize the auditory bullae. A sharp probe was used to pierce each bulla and disrupt the internal structures. During some

experiments, when the cat was already mounted in the stereotaxic frame a dorsal approach was used to visualize the posterior aspect of the bullae.

Clinically, labyrinthectomies are typically performed chemically by injecting an aminoglycoside antibiotic such as gentamicin into the middle ear transtympanically. These chemicals are ototoxic and cause irreversible damage to the hair cells. However, their effects are not immediate and can potentially cause renal damage which presents an unacceptable amount of risk from the perspective of humane animal care. Since the surgical labyrinthectomy was only performed during acute experiments after which the cat was euthanized, recovery and hearing loss was not a concern and thus was preferred over a chemical labyrinthectomy.

2.2.3 Muscle Dissection

Bone pins were inserted into the femur and tibia of both legs which were rigidly attached to the treadmill frame Figure 2.1. The leg is secured distally with an external clamp at the malleoli. The G, Sol, FHL, and Pl muscles were exposed and their distal tendon was cut. The free tendons were inserted into custom aluminum clamps which facilitate the interfacing with the experimental equipment. A chip of bone from the calcaneal insertion was preserved on G and Sol. The muscles were cleared of all fascia connections to prevent direct force transmission between the muscles being measured. Care was taken to preserve the blood supply and nerve innervation to all muscles. Saline soaked gauze was used to cover the exposed muscles and tendons to keep them moist.

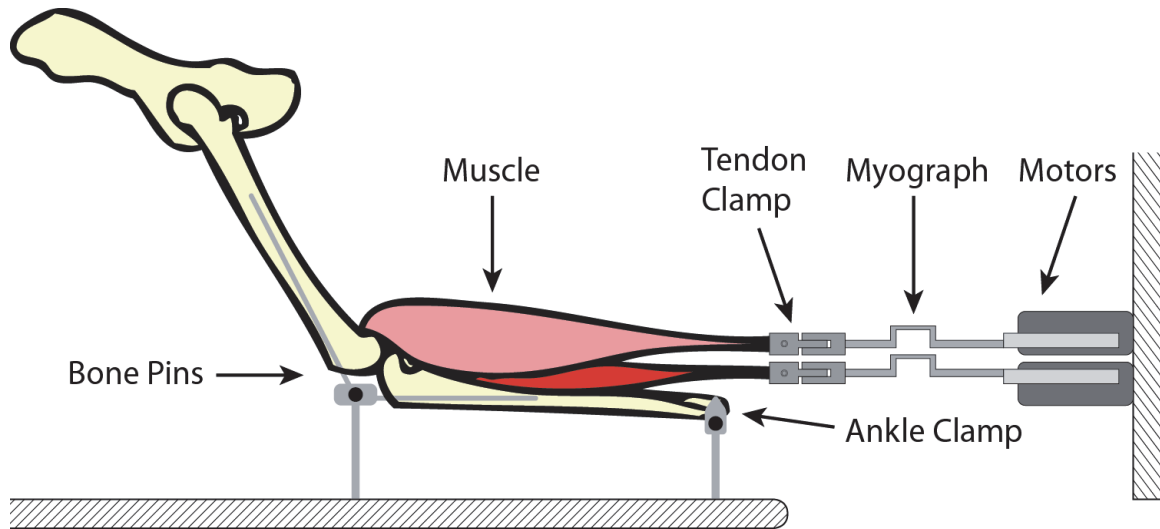


Figure 2.1 Muscle Puller System. Steel bone pins are inserted into the femur and tibia of each limb to be measured. The bone pins are rigidly clamped to a support frame over a treadmill belt. Muscles of interest are dissected so that they can move independently. The distal tendon of each muscle is affixed to a clamp which allows it to connect to linear motors with inline myograph force sensors.

2.2.4 Muscle Puller Apparatus

The tendon clamps from each muscle were attached to a myograph force transducer. The myographs consist of 2 semiconductor strain gages mounted on an aluminum beam. This was ideal because the high sensitivity of the gages allows for the accurate measurement of force without a significant deflection of the myograph. Since we were applying length based perturbations this was a critical design consideration. The strain gages were electrically matched and connected in a half bridge configuration which is necessary to keep their properties consistent regardless of temperature.

Each myograph was attached to a Parker 406LXR linear motor Figure 2.1. The motors were attached to a custom aluminum frame that allowed for each motor to be positioned independently. The motors were controlled by Parker Gemini GV6-U3 digital servo drives. Both the myographs and motor controllers were connected to a dSPACE

DS1103 PPC controller board which was running a custom real time program that both issued commands to the motors as well as collected force and length data. The real time program was running at 5 kHz, but data collection was downsampled to 1 kHz due to data bandwidth limitations.

The stretch paradigm used was a 2 mm stretch over 50 ms (a velocity of 0.04 m/s), a 100 ms hold period, and 2 mm release at the same speed. The 2mm length was selected because it is within the physiological range that the muscles normally experience (Goslow et al. 1973) and allows for a large number of repeatable stretches without causing harm to the muscle. In order to assess intermuscular effects, we used a paired stretch protocol where stretches of a single muscle, the recipient, was alternated with a coupled stretch with a donor muscle (Figure 2.2). An initial background force of approximately 3 N was maintained on all muscles to ensure that there was no slack in the muscle-tendon unit ensuring that the stretch perturbations and force recordings were accurate.

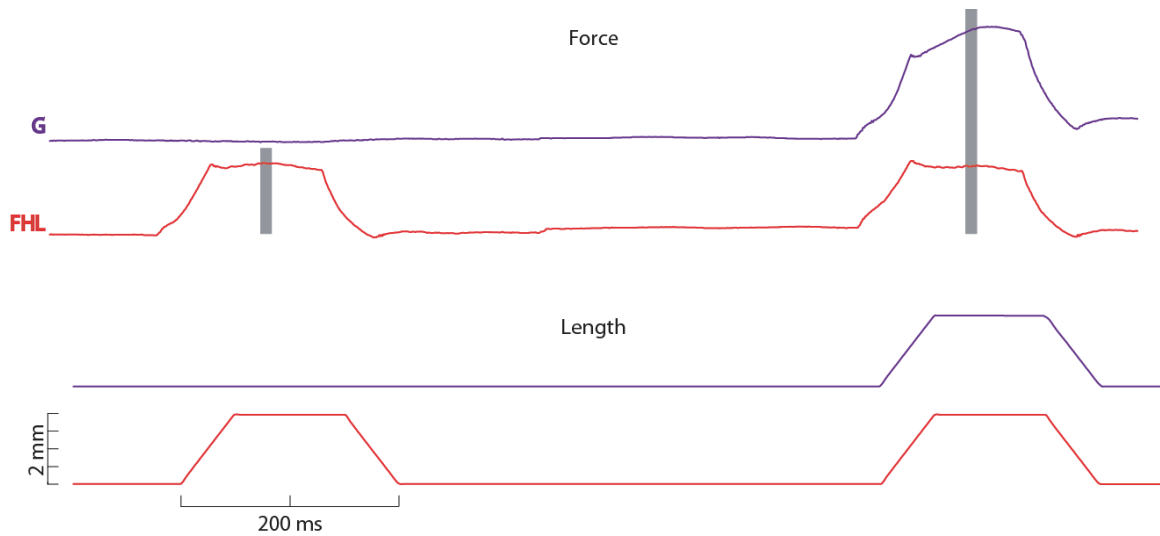


Figure 2.2 Force and Length Profiles. Each perturbation consists of a 2 mm stretch over 50 ms, a 100 ms hold phase, and a return to the resting position over 50 ms. The muscle designated as the recipient is first stretched alone and then simultaneously with the donor muscle providing intermuscular feedback. In this example, FHL is receiving inhibitory feedback from G.

2.2.5 Head Tilt

The angle of the head was controlled by a stepper motor the angle of which was recorded as an analog signal by the dSPACE system. The speed of the motor was limited to 3 degrees/s as it was discovered that higher speeds occasionally caused the cat to expire prematurely. Though unverified, the manner of the early expiration suggested that the spinal cord and remaining brainstem had become ischemic possibly due to emboli from the decerebration becoming dislodged and disrupting the blood supply in other locations.

Although based on the experimental paradigm developed by Gottschall (2007), neck angles of +/- 20 degrees were selected for the down/upslope conditions instead of the previously used 22.5 degrees. We found that in the upslope position of -22.5 degrees, the trachea became compressed and restricted respiration. Since it was vitally important

to ensure that any potential metabolic changes did not affect the results we were forced to reduce the angle used.

2.2.6 Locomotion and Crossed Extensor Reflex

In order to establish the force dependence of intermuscular reflexes we needed to perform stretches at a range of difference forces. In 13 cats we attempted to achieve this using the oscillating forces that occur during locomotion. Using the techniques developed by Ross (2006) and Stahl (2011) we were able to generate spontaneous stepping in preammillary cats with a combination of cutaneous stimulation at the base of the tail and manually moving the forelimbs in a locomotive pattern.

While locomotion is a highly relevant behavior, experimentally it does not always provide a wide range of force modulation. While in some cases the preammillary decerebrate cat will match its gait to a moving treadmill belt, they can also be insensitive to attempts to control the stepping rate. In these cases, where the stepping is very rapid, the frequency of the force oscillations makes it difficult to synchronize the stretches with the gait cycle.

An alternative method to generate a varying background force is to elicit the crossed extensor reflex (XER). In order to increase the force in the muscles of interest, all of which are ankle extensors, the contralateral tibial nerve was electrically stimulated (40 Hz, 0.1 ms unipolar pulse, $2T_{\text{voltage}}$) using a World Precision Instruments DS8000 stimulus generator and DLS100 optically isolated stimulation units. This mimics the effects of a painful cutaneous stimulus on the contralateral foot. This causes a withdraw reflex on the side that has been stimulated activating joint flexors and a corresponding increase in extensor activity in the opposite limb. The electrical stimulation was applied

continuously for 30 – 60 seconds during which the effect habituates leading to a gradual decrease in force back to baseline. Figure 2.3 shows data collected in the decaying phase of an XER response. By applying stretch perturbations throughout the course of the XER we were able to study the force dependence of the intermuscular reflexes over a broad range of force. In order to ensure that the XER was as consistent as possible between all tested conditions, we allowed the preparation to recover for 5 minutes between trials.

2.2.7 Data Processing

Despite all attempts to keep experimental conditions the decerebrate cat preparations could occasionally behave unpredictably. Thus, the first step in processing each trial was to crop out obviously inconsistent parts of the recording. During locomotion trials these inconsistencies often took the form of sudden and brief alteration of the gait pattern such as a temporary scamper. During XER trials, stretches were occasionally triggered prior to the background force being fully developed; to ensure consistency within the trial only stretches performed during the decaying phase were kept (Figure 2.3). All processing and analysis was performed using custom software written for the MATLAB environment.

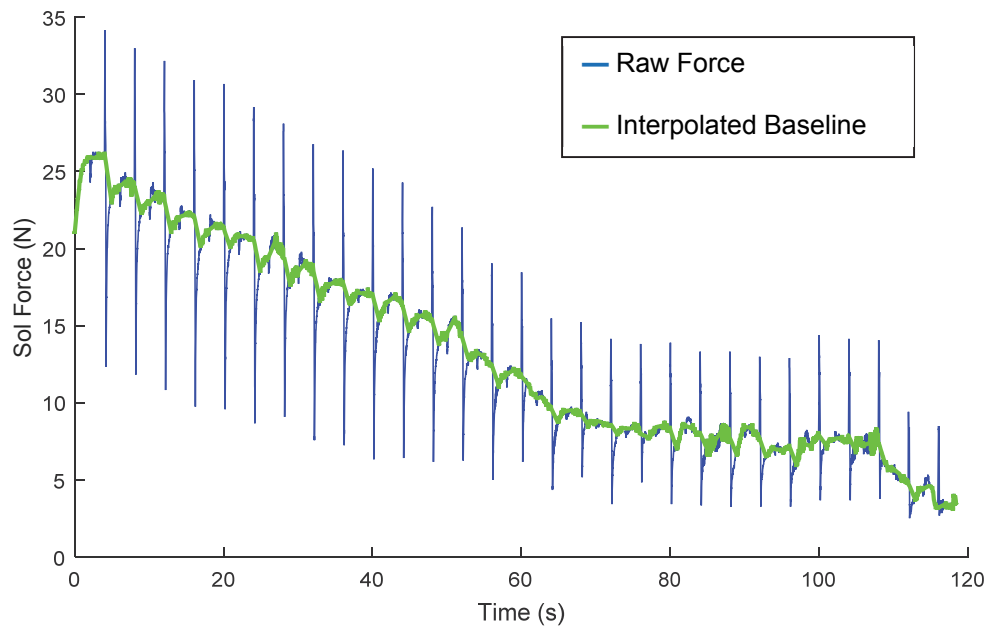


Figure 2.3 Raw Force and Interpolated Baseline. The blue trace is the raw force data from a recording during XER. At this timescale the individual stretch perturbations appear as spikes on in the raw force record. The green curve was created by replacing the stretch responses with a linear interpolation. This approximates the underlying XER curve.

Next, the force recordings were parsed into individual records of each stretch perturbation. For each individual force record the baseline force was calculated by performing a linear interpolation using the forces prior to and immediately after the stretch. This calculated baseline was then subtracted from the entire force record. This step was necessary because under normal conditions we expected the baseline force to be changing throughout the 200 ms of the stretch perturbation and in order to isolate the forces that are attributable to the muscle response independent of the changing background force we needed an estimate of how those forces would be varying during the stretch phase. The linear interpolation is especially suitable for XER as the decay phase

caused by habituation is approximates well to a linear relationship over the extremely brief duration of the stretch.

The resulting force records were further distilled down to 4 time points that represent different aspects of the reflex response. The earliest time point that we would expect to see any reflexive activity is at 12 ms, the minimum time needed for the monosynaptic stretch reflex. Thus, we used the force observed at 10 ms after the start of stretch as an experimental diagnostic; since any apparent effect that occurs at this time point cannot be attribute to neural activity it would instead indicate some sort of mechanical coupling.

We were also interested in 3 different time epochs of the force response: 30-70 ms, 70-110 ms, and 110-150 ms which we will refer to more simply as the early, middle, and late epochs (Figure 2.4). The early epoch represents the response due to the fastest pathways, the middle contains the effects to a blend of pathways of all latencies, and late epoch is representative of those pathways that have a long duration and have stabilized to a relatively static response.

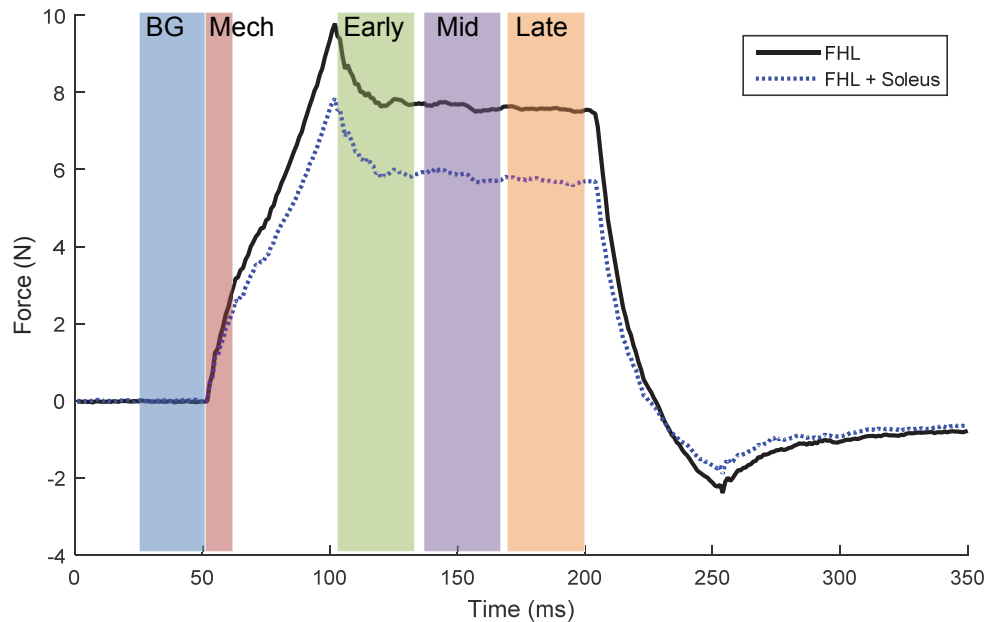


Figure 2.4 Force response curves are divided into different epochs. The blue shading indicates the phase prior to the stretch and is the background force against which the force responses are compared. The red area is the first 10ms after the stretch is initiated; any separation between states in this epoch indicates mechanical coupling between muscles as no reflex activity is fast enough to be present at this period. The green, purple, and orange areas represent the early, middle, and late epochs, respectively. These epochs cover the entire 100 ms hold phase.

2.2.8 Analysis

In order to establish the force dependent intermuscular relationship, we performed a 2nd order polynomial multiple regression on the force response (y) and the background force (x) of the recipient muscle with a dummy coded variable (S) indicating whether it was stretched in isolation or in combination with the donor muscle.

$$y = \beta_0 + \beta_1x + \beta_2x^2 + \beta_3S + \beta_4xS + \beta_5x^2S$$

Graphical, this takes the form of 2 parabolic curves fitted separately to the data that corresponds to autogenic donor responses and those with intermuscular feedback.

The regression was performed simultaneously so that the residuals could be used to

perform an F-test to establishing whether the autogenic and intermuscular data sets are statistically distinct. Our null hypothesis was

$$H_0 = \beta_3 = \beta_4 = \beta_5 = 0$$

Or in other words, that the coefficients of the second curve are insignificant enough that the parabola in the first curve is sufficient to describe both datasets. Rejecting this null hypothesis with a p value < 0.05 we can conclude that there was a significant intermuscular effect. Of course, as applied to the 10 ms time point where no spinal cord mediated intermuscular effect were expected accepting the null hypothesis confirms that there was no significant mechanical coupling between the muscles.

Although there is no direct correspondence between the terms of the polynomial and any physiological properties the parabolic fit was chosen because it matches the data extremely well. At high levels of background force, we even observed a decrease in response force possibly due to the muscle being maximally recruited. This phenomenon further reinforces the 2nd order polynomial as the ideal choice to describe the data.

2.2.9 Exclusions

After the completion of analysis some trials were excluded from consideration for a number of factors. In some trials we found that there were no reflex interactions between the donor and recipient muscle which was confirmed by the lack of statistical significance between the paired and solo stretches. There are numerous possible causes of this such as lingering anesthetic effect, but regardless of the source, without observable reflexes we would have been unable to make any determination regarding how they were modulated with head tilt.

There were also some cases, for both locomotion and XER, in which the background force range was very narrow or very few stretches were included in a trial. In these cases, the polynomial fits were extremely unsuited to the dataset and were thus unusable for analysis. Furthermore, while the cause of the poorly ranged datasets was not always obvious we were concerned that it could be an indicator that the preparation would not provide reliable feedback.

2.3 Results

We attempted to produce spontaneously stepping in 13 male cats. Of these, 3 produced no locomotor pattern and 2 expired before any relevant recordings were taken. Furthermore, 4 cats which did have some stepping activity did not display any intermuscular reflex interactions across all conditions. 4 cats produced both spontaneous activity as well the expected intermuscular interactions.

We used tibial nerve stimulation to elicit XER on 18 cats (5 male). 1 of these cats was a premammillary cat that was first used to gather locomotion trials. 5 were also used to collect stiffness data (as described in chapter 4) prior to being used in this paradigm. 1 cat was not subject to the labyrinthectomy procedure and was used strictly as a negative control. 1 cat expired prior to data collection and 7 either had no XER response to stimulation or did not display any intermuscular interactions among any of the tested pairings. 1 of these cases was due to a firmware malfunction in our stimulus generator which was providing a DC signal instead of the commanded pattern.

4 of 7 of the group that did not produce any responses had previously been used with the robotic apparatus where they showed no signs of abnormality. In order to

transition between the two experimental methods, the cats had to be reanesthetized while performing the muscle dissection. While this procedure required a shorter duration and was a less invasive surgery than the initial preparation and decerebration the state of these cats was clearly altered after coming off anesthesia the second time. In addition to the lack of muscular responses all 4 cats were either hyperventilating (>100 bpm) or were in apparent respiratory arrest.

2.3.1 G-FHL (inhibitory feedback is modulated by head tilt)

The most robust interaction was found to be feedback from G to FHL. Figure 2.5 shows the relationship found during locomotion with G as the donor and FHL as the recipient.

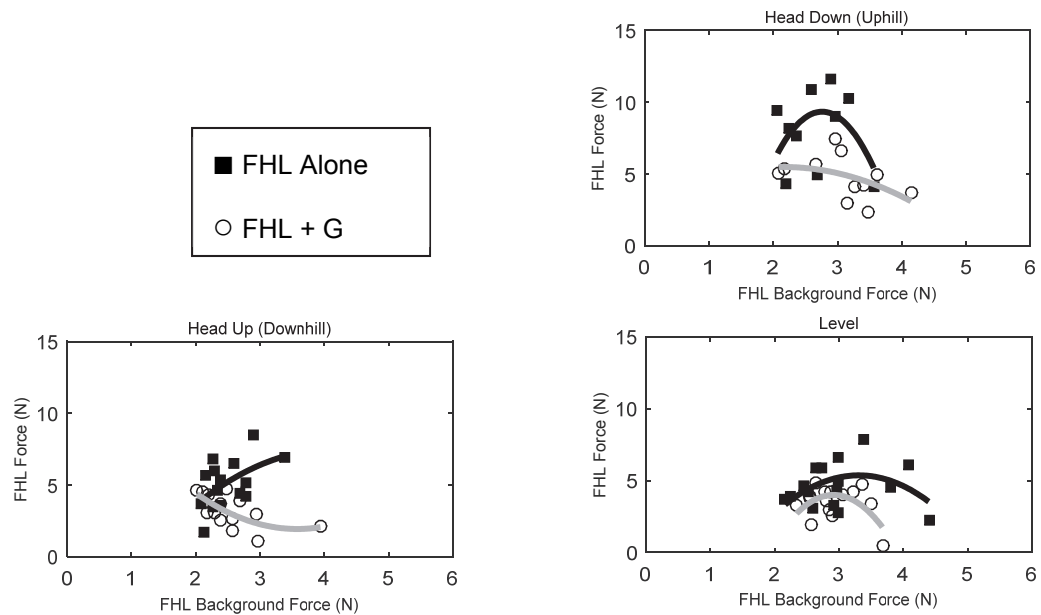


Figure 2.5 G inhibits FHL during locomotion. In the level condition, there is moderate inhibition from G onto FHL. This inhibition increases downhill condition (head tilted up 20°). In the uphill condition (head tilted down 20°) the inhibition is diminished to the point where there is no statistically significant distinction between the curves.

These data are from the experiment with the most consistent locomotion patterns and had the most consistent range of background forces between all 3 head tilt conditions. We found that in concert with our hypothesis that the magnitude of intermuscular inhibition increased as the simulated slope angle is decreased. This exemplar is representative of 3 of 4 experiments; the 4th experiment did not show any alteration in patterns between the head positions.

We additionally observed that the autogenic curves when FHL is stretched alone appeared to be sensitive to head pitch in 2 of 4 experiments. Seemingly in opposition to the change in intermuscular feedback, the autogenic response appears to be enhanced in the downslope condition and slightly diminished in the upslope. It is important to note that the increase in autogenic response magnitude and intermuscular inhibition magnitude do not scale together. This indicates that it is more likely that the pathways are being modulated separately and not by a single global variable or a system wide change in the state of the cat.

Trials performed with XER exhibited a similar trend of increased intermuscular inhibition from G to FHL in the head up condition in 6 of 9 experiments. 2 experiments did not show a change between head conditions and 1 did not have an adequate FHL response. Figure 2.6 demonstrates the similar progression of inhibitory feedback between head conditions.

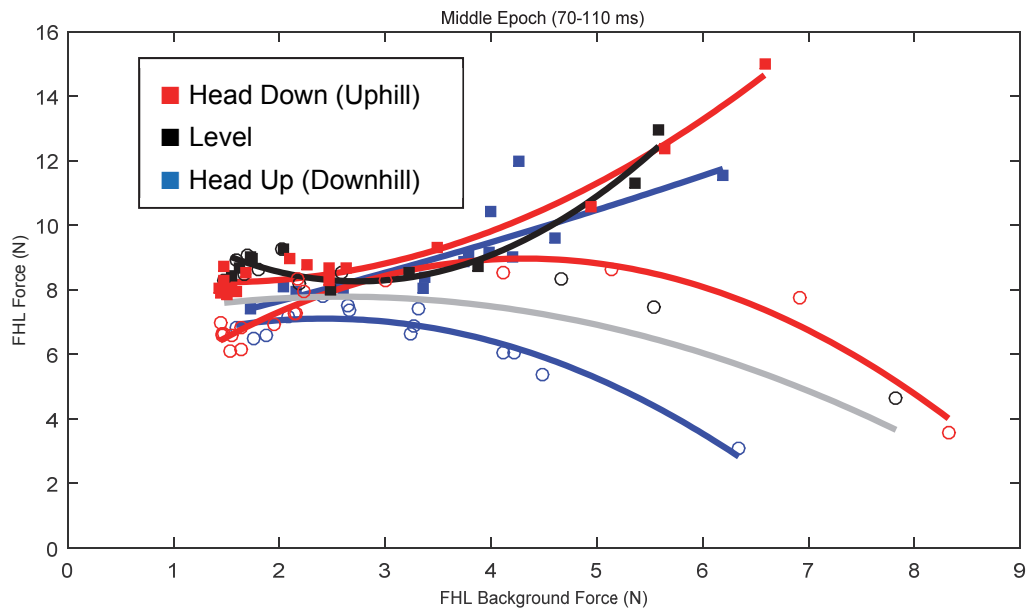


Figure 2.6 Comparison of intermuscular inhibition from G to FHL under XER. The square markers indicate FHL’s autogenic response which were very similar between head positions. The open circles show FHL’s response force when stretched with G. All head positions show that G provides inhibitory feedback to FHL, but the magnitude of inhibition increases with increasing head angle.

However, we also found that the head down condition did not consistently behave in this way. In only 2 experiments was there a clear decrease in inhibition for the upslope condition. There was 1 additional experiment where it appeared that the inhibitory feedback had been completely eliminated, but it’s not possible to establish with complete certainty that this effect was a result of the change in body orientation as this trial meets the exclusion criteria applied to other experiments. Unlike the experiments which were excluded, the apparent lack of inhibitory reflexes in this trial was not shared with trials in the same experiment and this it seems more likely than not that this is a true result.

In 3 of 9 experiments we found the head down condition to be the same as level and in 1 experiment the intermuscular inhibition from G to FHL appeared to be increased

as compared to level, although not as large as the head up condition. These mixed results make it difficult to fully confirm our hypothesis, but perhaps indicate that the relationship between slope angle and the modulation of feedback is more complex than a simple scaling of gain.

Figure 2.6 also shows that the autogenic responses were very nearly identical in all 3 head tilt conditions. This was the most typical result occurring in 6 of 9 experiments which is inclusive of the 2 that did not have any response to head tilt. The 3 instances where the autogenic curves were not perfectly matched did not correlate with any of the other observations, that is that it appeared to simply be a constant shift of both the autogenic and intermuscular curves for that condition. These data both agree and contrast with the findings from the locomotion trials in which the altered autogenic responses did appear to match head position but similarly did not seem to affect the intermuscular responses. One caveat to these findings is that in order to maintain a consistent baseline tension of 3N, the resting length of muscles had to be slightly increased intermittently. Unfortunately, this was unavoidable and necessary to have accurate force recordings.

2.3.2 FHL-G (modulation was not as consistent)

The trials which applied intermuscular feedback from FHL onto G were less consistent than in the opposite direction. The force responses from G were often slightly smaller than the other muscles tested. Considering that the G group is larger by far than any other muscle in the shank and has the ability to generate the highest forces, this finding was surprising. When considered as a percentage of activation, this means that G is being recruited at significantly lower levels than the other muscles studied. It is

possible that this lower level of recruitment is related to the inconsistency of results with G as a recipient muscle.

Of the 4 locomotion trials that were included for analysis, Figure 2.7 shows the only experiment that displayed the same relationship of increasing inhibition with decreasing slope as was found with the opposite pathway from G to FHL.

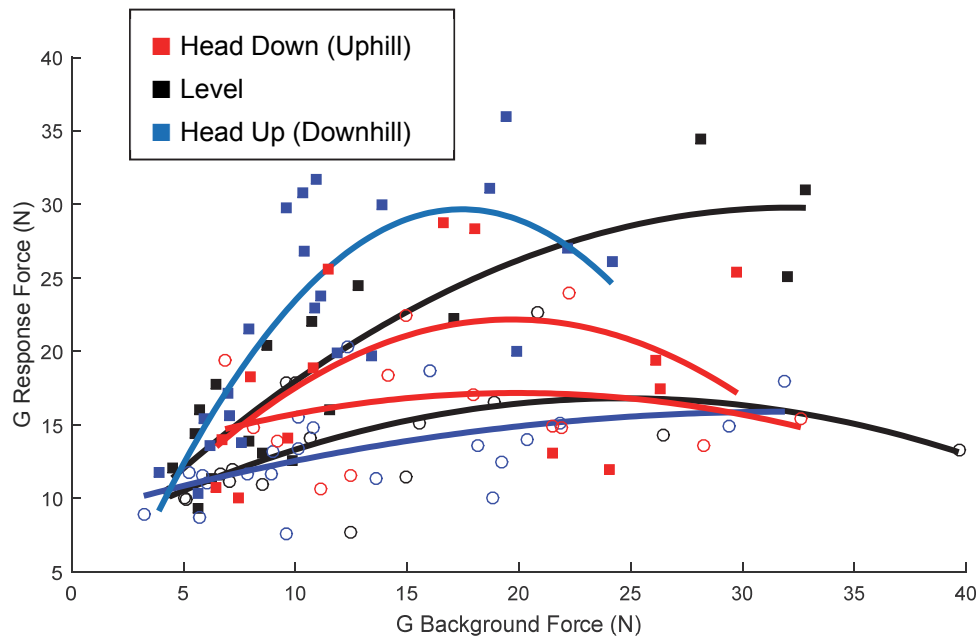


Figure 2.7 Feedback from FHL to G during locomotion. The square markers indicate autogenic G responses and the open circles represent the G responses when stretched with FHL. The feedback from FHL to G during locomotion shows increasing inhibition with increasing head pitch This mirrors the feedback in the opposite direction showing that G and FHL are mutually inhibitory and that their inhibition retains its symmetry over the range of simulated ramp angles.

The 1 experiment that did not show any alteration of feedback with head tilt in the G to FHL direction also did not have any effect from FHL to G. The other 2 experiments both showed increased inhibition in the head up condition as compared to level. The head down condition was the same as level in 1 experiment and had increased intermuscular

inhibition in the other. This variability somewhat mirrors the XER findings in the opposite direction in that the head down condition results appear to have a highly variable response to head tilt. The autogenic responses were not well matched between the head conditions, but unlike with the corresponding trials in the reverse pairing, there did not appear to be any trend with head position.

We had better results with XER as compared with locomotion, but the yield was not as good as with the FHL recipient counterpart due to G not responding to XER stimulation consistently. There were 2 experiments where G was not modulated at all by XER despite all other muscles responding normally. Furthermore, there was 1 experiment where the G did respond to stimulation, but the response was not sustained and decayed very rapidly over about 15s instead of the normal 30-45s. While this partial unresponsiveness to XER only occurred in about 1/3 of cats, G was almost always the muscle affected.

However, under ideal conditions we found that the head up condition exhibited enhanced inhibition in 4 of 7 experiments. In addition to the 2 experiments that were unresponsive to head tilt, 1 experiment showed the same level of inhibition between head up and level from FHL to G but a decrease in the corresponding trial from G to FHL. Figure 2.8 shows a progressive increase in inhibition with increasing neck angle and a well matched autogenic response.

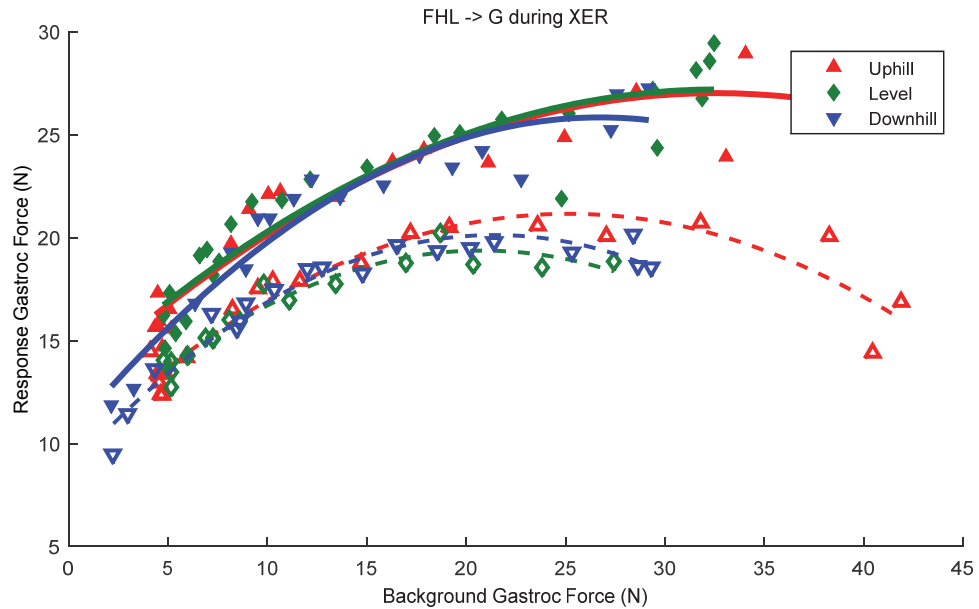


Figure 2.8 Inhibitory feedback from FHL to G during XER. The closed markers indicate autogenic G responses and the open markers are G responses when stretched with FHL. The inhibition from FHL to G during XER also showed a trend of reduced inhibition with increased simulated slope angle. G did not always respond to XER, even when its viability was confirmed by the feedback provided in the opposite direction to FHL.

Consistent with the other head down results, the hypothesized trend which is represented Figure 2.8 was only found in 3 of 7 experiments. 2 show no discernable difference against head level and 1 showed that the head level condition to have the least inhibition of the set.

Despite the more erratic nature of G's responses, the autogenic curves exhibit roughly similar properties as FHL: a mix of very well matched autogenic curves, but with a few that sporadically show a constant-force shift in the response magnitude. These changes do not seem to have any relation to the head position are possibly an experimental artifact.

2.3.3 G/Sol

Recordings performed using Sol were nearly as problematic as with G, but for virtually opposite reasons. Sol is a much smaller muscle than G and when splitting their shared calcaneal tendon much less remains with Sol than with G. This small tendon and muscle are much easier to damage during the dissection. This was exacerbated by the fact that Sol was usually the most agreeable to stimulation and showed high levels of activation before any others responded at all. This resulted in many attempted experiments with Sol ended with tendons broken or torn to the point that data could not be collected. This is, of course, entirely due to the experimental process and is in no way reflective of Sol's role or behavior in an intact cat.

Due to the problematic nature of these 2 muscles we were only able to achieve a consistent set of recordings in single experiment. Despite this we can see in Figure 2.9 that Sol is providing an excitatory intermuscular signal to G in all head tilt conditions. It should be noted that the head level condition did not meet our criteria for statistical significance between autogenic and intermuscular states with a p-value of 0.052 despite a clearly visible separation between the curves at higher forces. This is due to the poor separation of data that was collected at lower forces. However, seeing as there was no objective reason to exclude these data, we must accept that this result is not as reliable as some of our other findings.

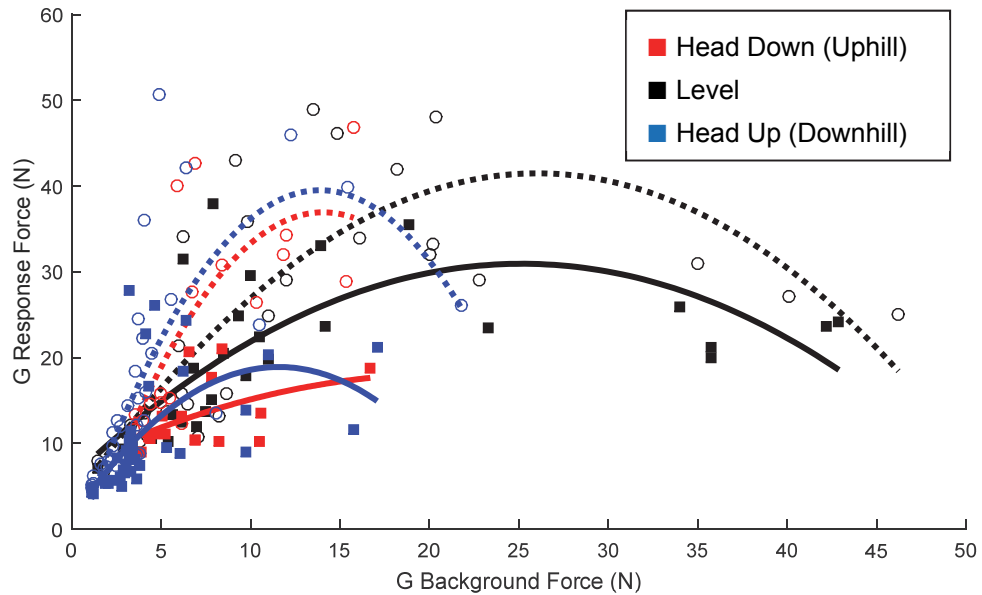


Figure 2.9 Sol provides excitatory feedback to G during locomotion. The closed square markers indicate the autogenic response of G and the open circles represent the G responses when stretched with Sol. The range of G background forces is diminished in the non-level conditions, but the excitatory feedback appears to be slightly greater with head tilt.

We can see in Figure 2.9 a number of differences between head conditions. Both the head tilt up and down conditions produced a much smaller range of background forces in G as compared to level, but also both showed a greater level of excitation over that range. Another important observation was that under all 3 conditions the relationship from Sol to G remained an excitatory one.

When this relationship is examined under XER we also find that Sol feedback to G always excitatory. However, this excitation did not seem to be modulated with head position. In 5 of 7 cases we found that all head positions exhibited an invariant relationship as shown in Figure 2.10.

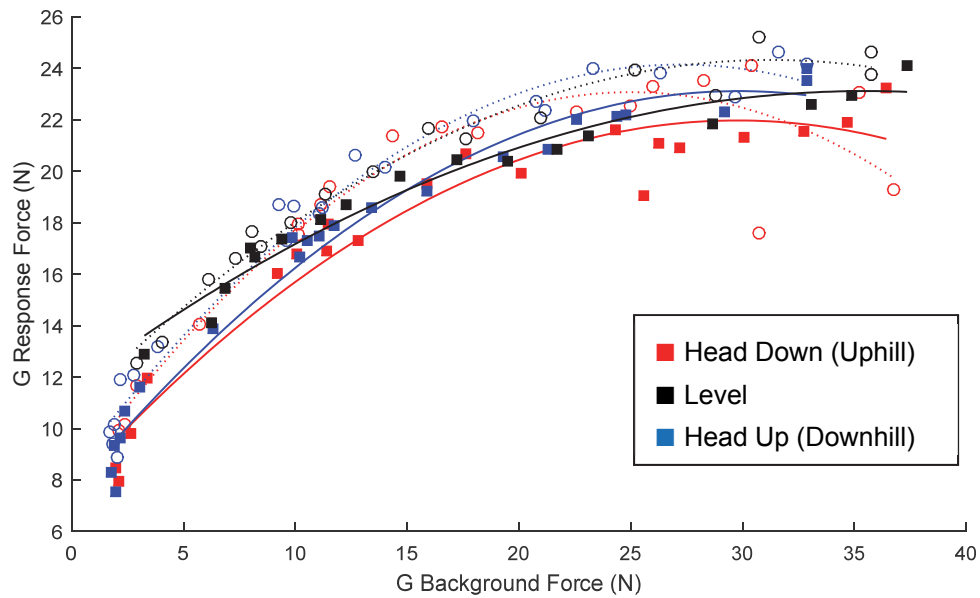


Figure 2.10 Excitatory feedback from Sol to G does not appear to vary with head tilt during XER. The magnitude of excitation appears to be smaller than what was observed under locomotion.

This included the 2 experiments that did not show head tilt modulation in the G/FHL combinations. It is interesting to note that the magnitude of excitation was greater in the case of locomotion as compared to what was observed with XER. Due to the small sample size no conclusive determination can be made, but this is potentially suggestive that XER and locomotion do not activate the same pathways for all muscle combinations.

The feedback from G to Sol was especially difficult to interpret. Not only were no clear trends found with respect to our variable of interest, there was a wide range of intermuscular interactions within experiments. We found both excitatory and inhibitory feedback being provided to Sol from G. It's possible that splitting the heads of G would help to elucidate the true nature of the relationship between Sol and MG/LG with respect to the body orientation signal, but we were unable to establish any trends in this study.

2.3.4 Control

In order to ensure that the changes observed between each head tilt condition was due to a change in the body orientation signal and not due to a mechanical linkage or disruption to the remaining brainstem we performed experiments that did not include the labyrinthectomy procedure. As shown in Figure 2.11 we found intermuscular inhibition reflex patterns that are identical between head tilt positions.

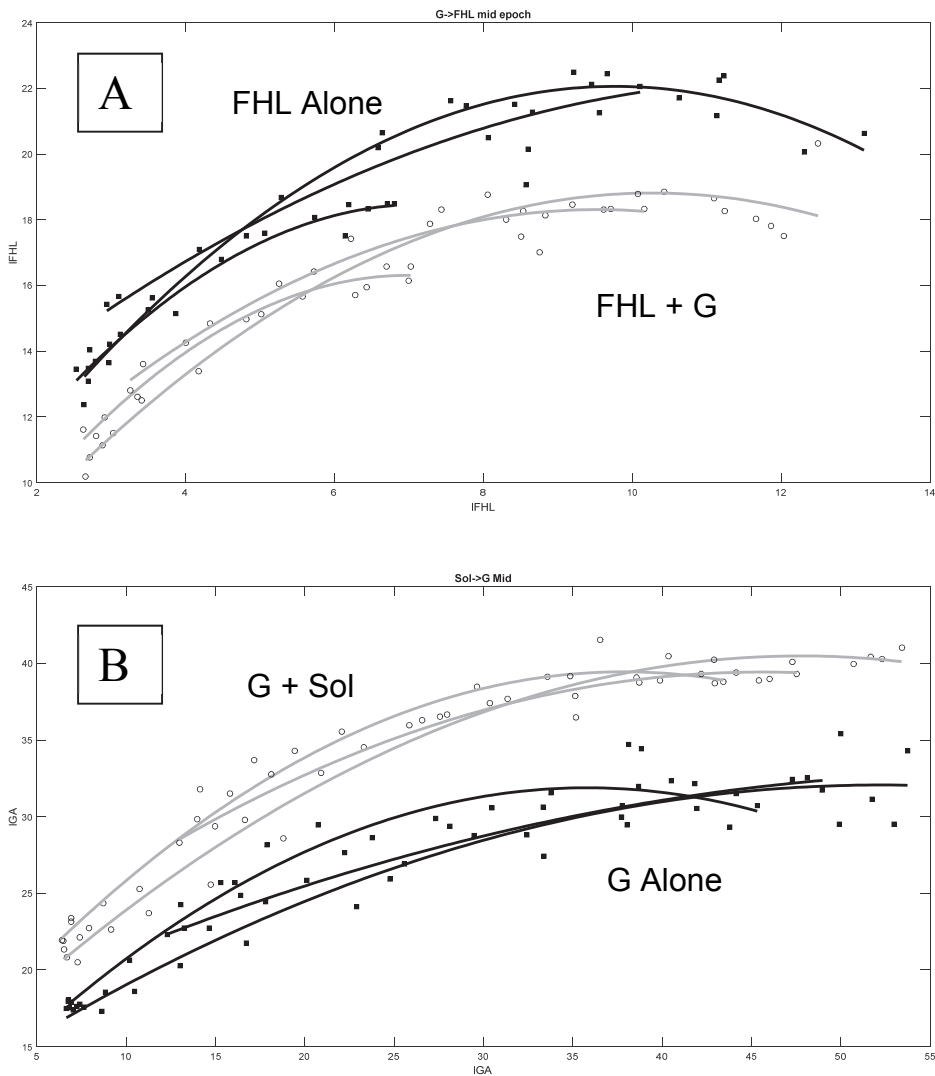


Figure 2.11 Control experiments with no labyrinthectomy show that reflex responses are invariant with head tilt. In both plots the solid square markers show the autogenic responses of the recipient and the open circles indicate the responses when stretched with the donor muscle. Plot A shows that all conditions produce the same level of inhibition from G to FHL and plot B shows the same for excitatory feedback from Sol to G.

As mentioned earlier, there were some results in experiments which did have the labyrinthectomy procedure but did not seem to be sensitive to head position. It is possible that the labyrinthectomy procedure was unsuccessful in these cases, but we did not have

an independent means with which to establish this. In the absence of any other verifiable explanation of these negative results, we must err on the side of caution and include them as legitimate result.

2.4 Discussion

The basis of our hypothesis that intermuscular reflexes would be the primary target of modulation in response to the body orientation signal is that not only do they provide coordination between muscles by its very nature, but also because it is known that these reflexes span multiple joints in the limb and thus have the capacity to have wide ranging effects similar to what are necessary to alter postural and gait patterns to perform different tasks. In this context, it is possible that the reason we find the most consistent exchange of proprioceptive feedback to be between G and FHL is due to the fact that they have much different mechanical actions due to their anatomy. In contrast, the feedback between Sol and G which have much more similar action and even share a tendon and insertion do not seem to have their intermuscular feedback strongly modulated by the body orientation signal. From the perspective of the task performance, the biomechanical contributions of G and Sol are partially redundant due to their shared tendon and thus neural coordination between the two may not actually be useful or necessary. While the activation patterns of G and Sol both vary with slope angle G is much more sensitive which may also be indicative of a lack of force dependent coordination (Gregor et al. 2006).

While we consider G to be mainly an ankle extensor owing to its origin on the femur it also has some contribution to knee flexion which somewhat weakens this theory. It is possible that if inter-joint coordination is the main function of the intermuscular

feedback changes caused by the body orientation signal then these changes would scale with the relative contributions by each muscle to their joint torques. In this case, the very small contribution of G to knee flexion would cause changes in feedback with Sol in amounts that are below the threshold of detection of our equipment.

Alternatively, it is possible that the relationship between ankle and toe actuators is the critical relationship that is being modulated. While the forces produced by every muscle in the entire leg has some effect on the mechanics of the leg, there is a distinct difference in role and function that shifts from proximal to distal segments. The largest and most powerful muscles which are responsible for most of the propulsive force are on the most proximal limb segments. This configuration minimizes the rotational inertia of the limb which improves the energetic efficiency of limb movements. The corollary to this is that the muscles with distal insertions have smaller physiological cross-sectional areas resulting in lower force production capacities (Prilutsky and Zatsiorsky 1994) which could be advantageous for finer positioning of the distal limb. Due to this organization, it could be possible that our finding that intermuscular feedback modulation is greater with FHL, a muscle with an extremely distal insertion, is reflective of a strategy which prioritizes the distal segments to achieve the altered motor patterns needed for sloped walking or standing. The fact that this pattern cannot be accounted for by muscle size (Lyle and Nichols 2018) or GTO density (Banks et al. 2009) also support the idea that function dictates this organization.

Our findings show that while head tilt did cause some autogenic changes, there was not a consensus in the results that indicate that this was not a strong relationship. Autogenic alterations to head tilt were also studied by Ross (2006) in locomoting

decerebrate cats. This study did not use the labyrinthectomy procedure and were therefore not able to obtain results over a large range of background forces. This difference in technique doesn't not readily explain the differences in our findings and theirs. Where we found that the autogenic gain of FHL increased with head position during locomotion, Ross observed the opposite relationship. Although our data do not provide an example, it is possible that the autogenic curves could overlap in such a way that at lower background forces Ross's observation is seen while over the entire range of background forces that our findings dominate.

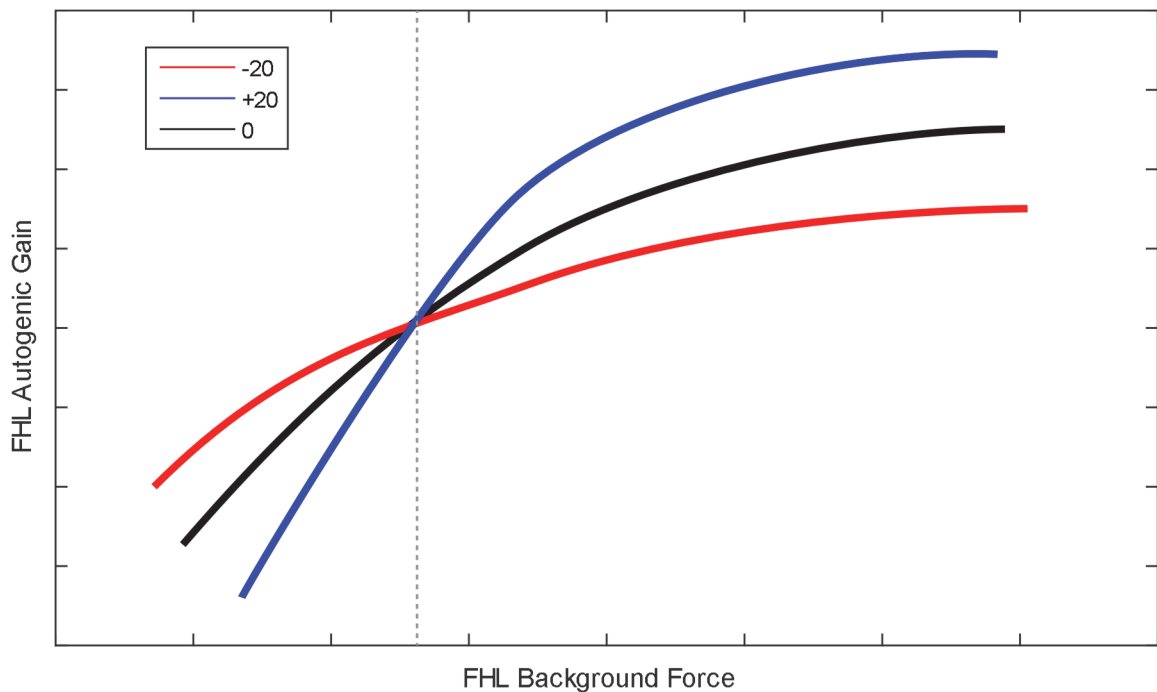


Figure 2.12 Theoretical extrapolation accounting for apparent reversal of head tilt relationship. The autogenic curves of FHL appear to have the opposite trend in this study as compared to what was reported by Ross (2006). The range of background forces was different between the two studies and this graph demonstrates an example of curves that could account for both findings. If the curves intersect near the background force indicated by the dashed line, the progression between head positions appears to be opposite on either side of this intersection.

Perhaps of greater interest is our finding that the autogenic curves typically did not change during XER while they did during locomotion. This is potentially indicative of 2 different strategies being implemented by the nervous system to achieve similar task dependent alterations. The simplest explanation for our findings is that the tuning of autogenic reflexes to the body orientation signal only occurs during locomotion, whereas the modulation of intermuscular reflexes occurs during all conditions.

The other major trend that we discovered was that the head up condition had much more consistent results than with head down. This is somewhat corroborated by Ross's finding that the head down condition caused an increased variability in autogenic G force responses as compared to the other positions. It is possible that the cause of this inconsistency is that there are multiple strategies that can be employed for successful uphill mechanics and perhaps modulation of shank muscles is not necessary to achieve the task. Furthermore, while we assume that the animal will tend to shift its posture to position its center of gravity towards the middle of its base of support, this is not strictly necessary to maintain balance on a sloped surface. For example, a 4-legged table, with no ability to adapt to its environment, can successfully remain upright on sloped surfaces within a certain range. It is possible that in some cats, a critical threshold of uphill input must be met before a new strategy is adopted and this threshold might vary between cats or be dependent on experimental factors such as the decerebration or brainstem transection.

We also found a number of cats which did not respond to head tilt and displayed the same patterns as our control data. There are 3 possible scenarios that explain these findings. The first is that these are true counterexamples against our hypothesis and show

that the cat sometimes does not alter its reflex patterns in response to head tilt. This is the scenario that we have accepted for this study for the sake of scientific rigor as we cannot definitively prove any of the alternate explanations.

The second possibility is that the labyrinthectomy procedure was unsuccessful in these cats. As was discovered by Gottschall (2007), the modulatory effect is transient in decerebrate cats with intact vestibular function and we would thus have not been able to capture the effect over the typical 60 s duration of our recordings. Given that no modulation was found in either leg for any muscle combinations, it seems very likely that a global experimental error like this to be the cause. While it is technically possible to independently assess the vestibular activity of the decerebrate cat we determined that the logistical burden was too great and put each experiment at an even higher risk of failure. The caloric reflex test uses warm and cold water, irrigated via the external ear, to stimulate the vestibular system and cause a horizontal nystagmus. This is due to the altered temperature causing convective currents in the endolymph causing illusory vestibular signals. In theory, our cats with proper labyrinthectomy should have no response to the temperature change since the vestibular structures have been destroyed. However, this test cannot be performed under anesthesia since it relies on the vestibulo-ocular reflex which would be suppressed by isoflurane. Thus, in order to properly examine the cats for vestibular function, the caloric test would have to have been performed prior to the experiment on awake cats which creates a potentially stressful environment for the cat and a hazardous one for our laboratory personnel. Additionally, the caloric test would have to be performed a second time after the decerebration which would require the head to be removed from the stereotaxic frame. Since the decerebrate

cat can be very active when not anesthetized, allowing the head to be unsecured presented an unacceptably high risk. It is possible that a redesigned stereotaxic frame that does not rely on ear bars could allow this test to be performed, but we did not have the resources to attempt this.

A third possibility is that the decerebration and brainstem transection were also responsible for disrupting the transmission or integration of the body orientation. If this is the case it would be analogous to the cats which experienced respiratory arrest immediately following decerebration which we attribute to brainstem damage. In addition to our direct manipulation of the brainstem, there is a strong possibility that the cat has a large systemic immune response which is typical of major head trauma. It is possible that inflammation could be severe enough to cause secondary injury to the centers that integrate the body orientation signal from the various sensory inputs or the spinal pathways that transmit them to the circuitry responsible for the modulation of muscular reflexes. It seems incongruous however, that an immune response, that we should expect to happen in nearly every case, could cause these relatively rare events. However, it is possible that the nature of the open craniotomy normally prevents pressure build up on the brainstem and spinal cord in all but a few instances.

While the experimental inconsistencies apparently in this study might suggest that more animal experimentation is necessary before translating to human studies, performing a similar study on human patients may actually help to control for some of our potentially confounding factors. The 2 biggest weaknesses of our study design were the longevity of the decerebrate preparation and the inability to independently verify the labyrinthectomy procedure. A supplemental study could be performed on human patients

who have received therapeutic labyrinthectomies or vestibular neurectomies as a treatment for vestibular disorder such as Ménière's disease. With the visual field controlled with a blindfold, these subjects should respond to head tilt in a similar fashion as the decerebrate cat, but without the complications that rise from the highly invasive surgeries. Of course, it would not be possible to get an equivalent level of detail regarding individual muscle interactions but results from this human study might be useful to aid in the interpretation of our findings.

It is worth noting that the absolute changes in intermuscular feedback in all cases is very modest ($<4N$). Despite this, it is important to keep in mind the muscle pairings that are examined in this study, while hopefully representative, are only a small fraction of the possible donor sources of proprioceptive feedback. One can reasonably infer that in totality these small changes in the exchange of feedback yield a significant alteration of limb mechanics. While our findings did confirm our hypothesis that intermuscular feedback would lead to increased inhibition during downslope conditions and partially confirmed the converse we were also interested in determining how these small changes combined to alter the mechanics of the whole limb.

CHAPTER 3

ROBOTIC SYSTEM DEVELOPMENT

3.1 Introduction

Translating platform apparatuses have been employed to study postural responses in quadrupeds in multiple investigations. One of the earliest implementations used a hydraulic cylinder to produce translational perturbations of a support surface (Mori and Brookhart 1968). This system was intended for use with intact dogs that were trained to stand still and was limited to perturbations along a single axis. The design used by Macpherson (van Eyken et al. 1987; Macpherson 1988) included a second rotational hydraulic actuator to allow for radial displacements at arbitrary angles. This system was also designed for the use with awake, trained animals and it was noted that the selection of hydraulic actuators was partly to minimize the audible noise which might have startled the animals. It was also noted that while the design choice to use a rotational joint instead of 2 translational joints allowed for a simplified control schema as the joints never need to be actuated simultaneously to produce the desired radial platform perturbations.

The Macpherson system was recreated using electric motors for the use with decerebrate cats by Honeycutt et al. (2009). The noise generated by leadscrew motor used to actuate the translation joint was not a concern since the decerebrate cat is unable to process sounds. An additional feature included in this iteration was the ability to set each paw support to move with the platform or to remain stationary. This allowed for the ability to measure individual limb stiffness in the horizontal plane.

While these systems were critical to provide the foundation of our understanding of how mammals maintain posture they are limited to 1 dimensional perturbations in a

fixed plane. And while it may be conceptually convenient to describe biomechanical actions in a single anatomical plane it is well established that a full 3D description of these motor programs is necessary to understand how the limb interacts with the environment (Lawrence and Nichols 1999; Lawrence and Nichols 1999). It was our goal to eliminate these constraints by designing a robotic system using commercial 6-axis robotic arms. Robotic arms were previously deployed by Perreault et al. (2002) for use with anesthetized cats. In this study the robot arm was used to produce rotational perturbations around the ankle joint. Based on this successful implementation we selected robot arms with similar specifications for our system (the model used by Heckman (2008) was no longer in production.)

3.2 Methods and Results

3.2.1 Equipment

3.2.1.1 Robots

A set of 6 degree of freedom industrial robot arms were the obvious choice in designing this system because they are capable of manipulating the end effector into any arbitrary position and orientation needed. This flexibility allows for the implementation of our stiffness testing system, but also provides the capacity for additional features to be created in the future without having to change the underlying hardware. The Staübli Robotics AG TX-60 was selected as it was the model that replaced the RX-60 robot that had been previously used by Perreault et al. (2002) for use with the cat. The main difference between the TX-60 and RX-60 was that ac motors were used instead of dc motors. Thus, it was necessary to reevaluate these robotic arms prior to ordering to verify

that they did not produce electrical noise that might interfere with recordings. These robots are able to produce precise movements that are repeatable within 20 μm which is 3 orders of magnitude smaller than the movements that we used in this project.

Additionally, all joints and access points are sealed against liquid and dust infiltration which is a critical feature in the laboratory environment.

3.2.1.2 Force/Torque Sensors

In order to record the endpoint force and torque of the cat's hindlimb, load cells (ATI Industrial Automation Mini40) were attached to the end effector of the robot arms. These sensors were previously used by Honeycutt (2009) in a 2D platform robot and were repurposed for use in our system. In addition to having an appropriate range and resolution, the stiffness of the sensors is over 10^7 N/m which is much greater than the stiffness we intend to measure. To protect the load cell from biological fluids, a milled aluminum shield was mounted to the surface which extends down the sides. It was discovered that without this, residue could accumulate between the sensor cover and body and prevented accurate measurements. The manufacturer produces water and splash resistant versions of the same sensor, but since the damage was not caused by moisture infiltration, but rather the residue left behind, these options did not offer an adequate solution.

3.2.1.3 Motion Capture

Motion capture and EMG recordings were performed with a Vicon MX system. The system uses 6 high speed cameras which can capture up to 250 frames per second

and has 64 channels of analog inputs that are synchronized with the cameras. The sampling rate of the analog system can be increased to over 20 kHz on a reduced number of channels. This study used only up to 14 channels which leaves capacity available for future development. The Vicon MX system also has the capacity for other devices such as digital video cameras or force plates which were not implemented for this project but is important to the modularity of the system allowing for customization and expansion.

3.2.2 System Integration

The data collection and control of these systems was coordinated via various interconnections between these systems and a PC running LabVIEW and Vicon Nexus. The raw analog data from the load cells was first converted to force and torque signals using a custom microcontroller programmed with a calibration matrix provided by the manufacturer. The force and torque data were then transmitted digitally to the robot controller (Stäubli CS8C) via the fieldbus input using the CANopen protocol. This ensured that the force and torque data are always synchronized with the robots' positions. While synchronization was the ultimate requirement, this configuration allows for the potential of force feedback control of the robot without relying on connections to either of the other systems.

One limitation of the robot system is that due to the unique software architecture, the sampling rate for both the robot position and force data is functionally fixed at 250 Hz. While this sampling rate was found to be adequate for stiffness measurements, this limitation could have been overcome by bypassing the provided operating system (or writing a new one) and writing our software in assembly code, but this would have increased the complexity of development with no clear immediate benefit.

The 2 robot controllers are connected to a PC via a private local area network. LabView (National Instruments) was used to create a user interface, issue commands to the robots, and save the robot and force data to disk. The same PC uses a separate network controller to connect to the Vicon MX system which streams motion capture and EMG data to the Vicon Nexus software suite which can then be written to disk.

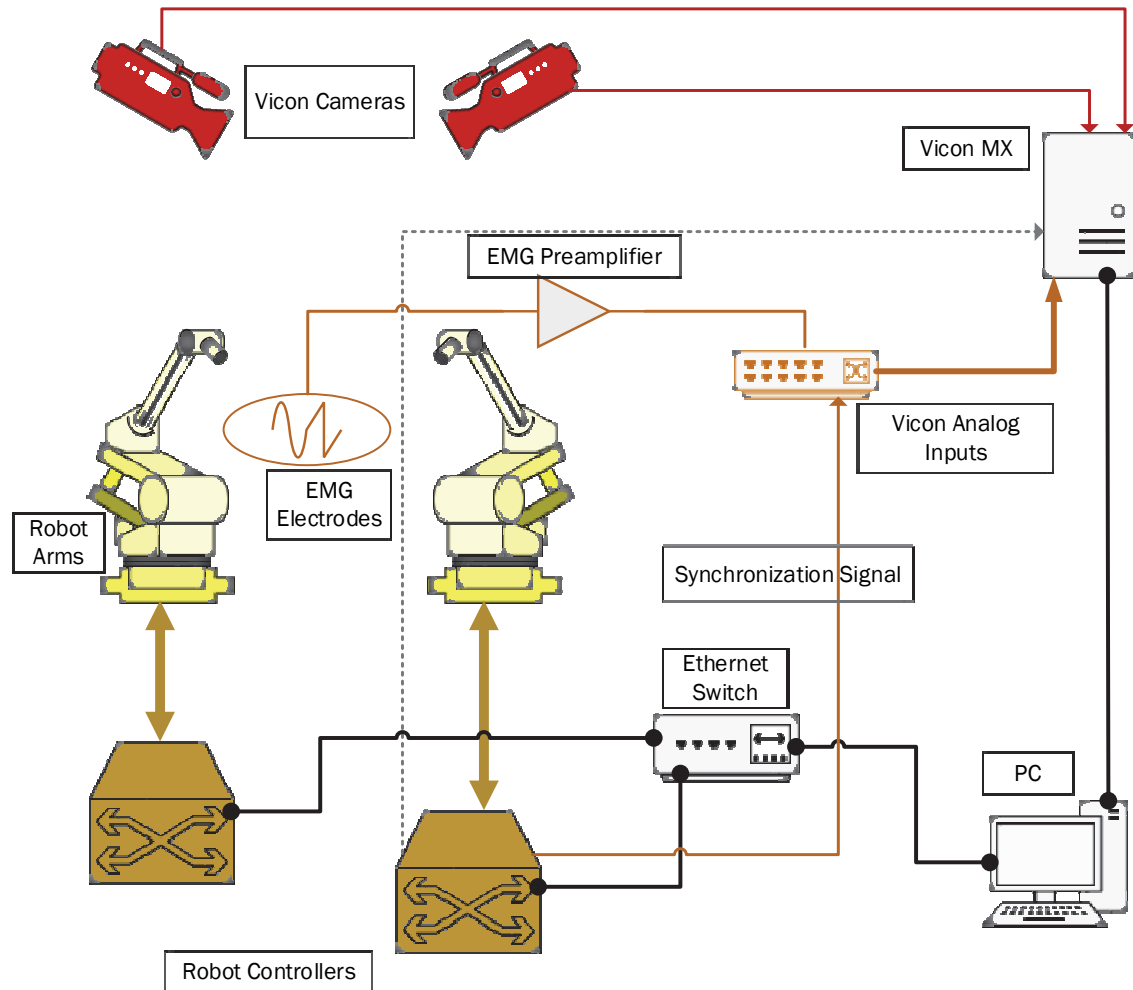


Figure 3.1 Schematic of the robotic stiffness measurement platform. The robot controllers use a CAN bus to sample data from the force/torque sensors (not pictured). Instructions for each perturbation are sent over ethernet and the results from each perturbation are sent back to the PC after each perturbation. An analog signal is sent from one of robot controllers to the Vicon system which allows for the synchronization of the robot and force data with the EMG and kinematic data.

The typical program flow is as follows:

1. User defines a set of perturbations to be performed via the LabVIEW interface and begins execution.
2. The position and timing instructions for the 1st perturbation are transmitted to the robot controller via Ethernet including an instruction to begin Vicon recording.
3. The robot controller sends a command to the F/T microcontroller via the fieldbus to trigger the Vicon MX system to initiate recording in the Vicon Nexus software.
4. The robot controller commands the robot arm to perform the specified perturbation; position, force, and torque data are stored in the controller while the perturbation is executing.
5. A binary signal from the controller's fast analog output indicating the start of the robot movement is sent to the Vicon MX analog input so that the data between the 2 systems can be synchronized offline.
6. At the end of each perturbation, the robot data is transmitted via Ethernet to LabVIEW which then saves it to disk.
7. The remaining perturbations are performed in the same fashion, but with the Vicon system recording continuously throughout.
8. The final perturbation includes the instruction for the Vicon recording to stop; this is carried out in the similar fashion as the starting signal.

3.2.3 Spatial Sampling Pattern

During the development of this system for the measurement of hindlimb stiffness in the decerebrate cat multiple modalities of perturbation patterns were developed. The

main motivation behind the development was to minimize the total duration of sampling without sacrificing accuracy.

3.2.3.1 Clockface and Rotate

The clockface and rotate paradigm was adapted from the planar sampling pattern used by Honeycutt (2009) which made radial perturbations at evenly divided angles. Most frequently 30° sections were used which resulted in 12 samples per run which is the source of the “clockface” moniker. To bring this method into 3 dimensions, we divided both the azimuth and elevation coordinates into an integral number of sections; perturbations were performed with a constant displacement from the origin to the target coordinates.

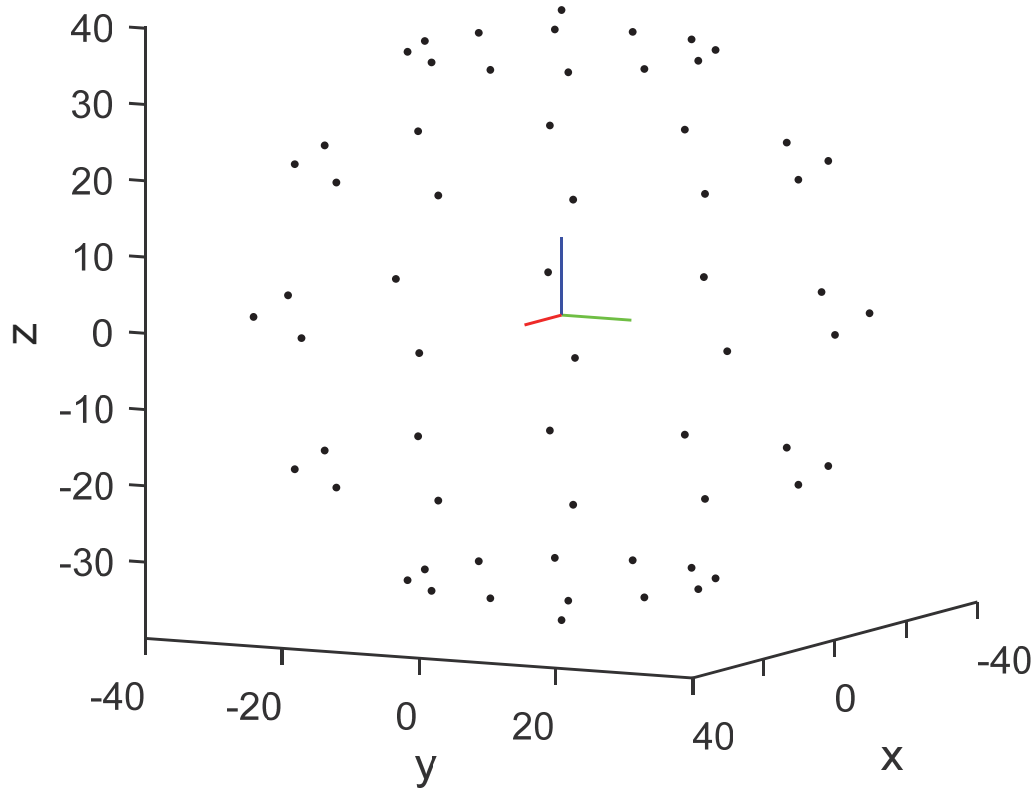


Figure 3.2 Diagram of the Clockface and Rotate pattern. This technique yields a sampling pattern of intersecting circles. While this grid pattern is intuitive due to its similarity to the latitude/longitude system used in cartography, the distribution is biased towards the poles of the z-axis. While an evenly distributed sampling pattern is not necessary for the accurate calculation of limb stiffness, oversampling at an arbitrary position results in unnecessarily lengthy collection times.

The benefit of this style of sampling is that it is conceptually similar to the studies performed in 2D and if factors of 180 are used, the perturbation directions are all performed at angles of integral degrees. Additionally, with the exception of the vertical poles, the sampling is performed in a grid pattern which has unique benefits in terms of graphing and compatibility with many of MATLAB's matrix based functions.

However, unlike in a 2D plane, this method does not create a set of uniformly spaced directions. Not only is the spacing between points uneven, but the sampling is spatially biased towards the vertical poles. This bias is extremely obvious at the poles (elevation of $\pm 90^\circ$) where all desired azimuth angles generate perturbations to the exact same point. Furthermore, only carefully selected divisions of the azimuth and elevation coordinates result in directions that are coincident with the cardinal axes which limits the flexibility of this method.

3.2.3.2 Equispaced

Mathematically, only sets of 4, 6, 8, 12, or 20 points can be perfectly distributed around the unit sphere as these describe the vertices of the 5 platonic solids. However, there are algorithms which can approximate evenly spaced points for an arbitrary number of points. We used LabVIEW to generate a user-specified number of points that are approximated equally spaced based on the golden section spiral algorithm.

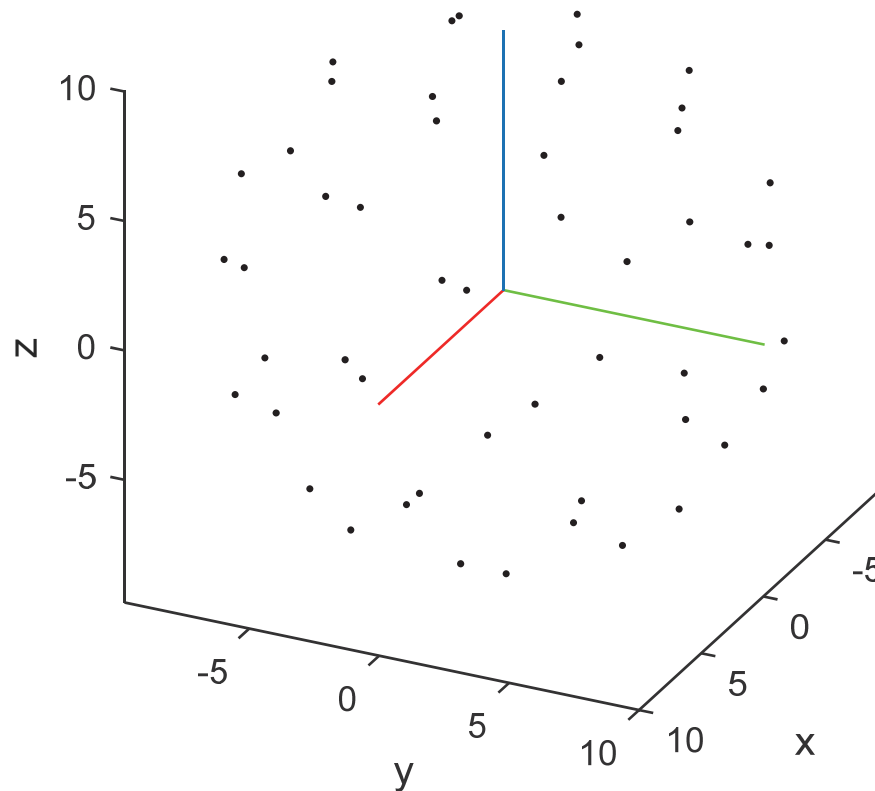


Figure 3.3 Example of 50 perturbation directions approximately evenly distributed. The golden spiral method is used to generate these points as it can be used with arbitrarily selected totals. Perfectly distributed points can only be achieved with specific totals that correspond to the vertices of Platonic solids. Evenly distribute perturbations are preferred for initial measurements as a poorly distributed set could introduce bias to the calculated stiffness ellipsoid.

The strengths and weaknesses of this technique are essentially the opposite of the clockface and rotate method. While the spatial pattern is as unbiased as possible, the lack of a grid pattern prevents the usage of many graphical techniques which rely on creating polygons from the sampled points. The spiral method also precludes the possibility that sampling will be performed in any of the typical planes used in 2D studies.

A more critical flaw was that in our initial testing using these two methods, we were not able to detect any changes between any of the head tilt conditions of the decerebrate cat. It seemed like the main problem was ensuring that the background forces at each sampled direction were similar enough to ensure that we were accurately representing the true stiffness properties. The XER technique used in the muscle puller system while producing a consistent force pattern generates a decaying level of background force. In order to adapt this to the robotic system, we attempted to combine data from multiple passes to decrease the range of background forces over the perturbation set, but this too did not demonstrate any consistent trend between head conditions.

3.2.3.3 Single Direction

One consistent result that we did find in our initial testing was the major axis of stiffness seemed to be aligned with the leg axis from the hip to the toes. Based on our findings in Chapter 2 that inhibition was enhanced in the head up condition, we hypothesized that head down condition should cause a corresponding decrease in stiffness for the whole limb. Based on this hypothesis, we expected that the major axis of stiffness should thus show the greatest magnitude of change and would thus be the location at which changes due to head tilt would be the most easily observed.

Based on this we created a set of perturbations that were all directed at the hip of the cat. The major drawback of this sampling pattern is that the 3D stiffness relationship cannot be established. However, this did allow us to simplify the analysis by averaging the force responses and using a straightforward Student's t-test to examine the statistical separation between the head conditions.

Additionally, in order to slow the habituation of the XER we injected DOI (2,5-dimethoxy-4-iodoamphetamine) intrathecally. This roughly doubled the duration of the XER response providing a 60s window with which to perform perturbations. With this extended window and the perturbations limited to the major stiffness axis, we were able to confirm that head tilt did cause measurable changes.

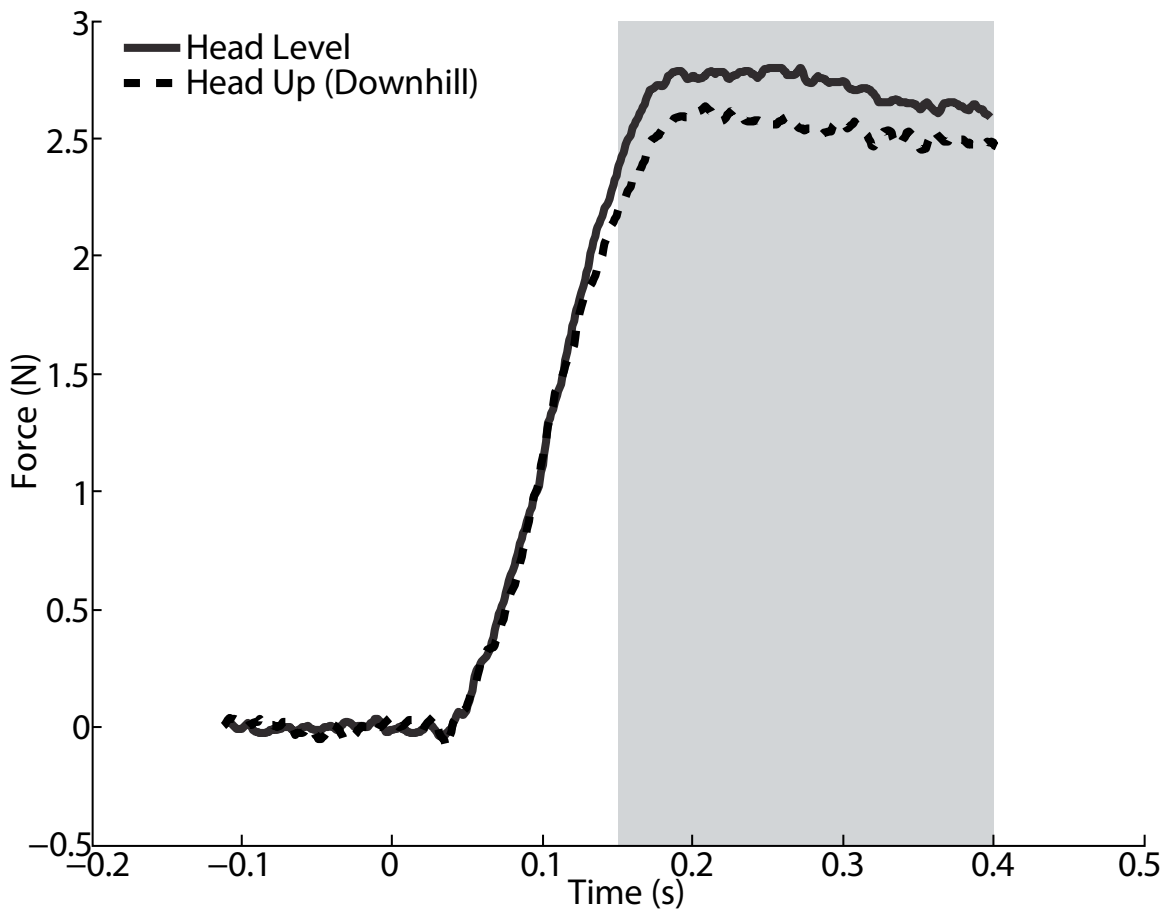


Figure 3.4 Using a single perturbation direction, whole limb force responses were collected during XER and the average force magnitudes were plotted. Student's t-test was used to determine that the downhill condition showed a statistically significant reduction in scalar force response in the shaded region. This confirmed that head tilt does produce whole limb biomechanical alterations and that these changes could be measured with our equipment.

While the single direction technique validates our system's ability to detect the limb mechanical changes caused by head tilt, the single axis measurements are insufficient to answer any questions regarding how these changes are made by the nervous system. While Figure 3.4 shows a significant reduction in force response when the head is tilted up this change has 2 mutually nonexclusive interpretations: the size of the endpoint stiffness ellipsoid has decreased and/or the ellipsoid has rotated. Despite this uncertainty, the single direction method demonstrated that our previous inability to detect changes with head tilt were due to the changes in force response were obscured by the variability introduced by XER.

3.2.3.4 Dynamic Major Axis Search

In order to fully capture the 3-dimensional endpoint stiffness ellipsoid changes we needed a sampling method that was adequately dense to provide an accurate measurement yet rapid enough to capture a consistent state of the decerebrate cat. To achieve this, we adapted a technique that is commonly used in image compression: bias spatial resolution towards areas that have rapidly changing content. Based on our findings with the clockface and rotate and equispaced techniques and results of prior studies (Mussa-Ivaldi et al. 1985) we can reasonably assume that the stiffness properties of the limb will be geometrically ellipsoidal and nearly a prolate spheroid. Thus, the location at which the limb response forces are changing the most rapidly are at the poles of the major axis of the stiffness ellipsoid.

To exploit this knowledge, we created a triphasic sampling method that dynamically biases the sampled perturbation directions towards the poles of the stiffness ellipsoid. The first phase performs a quick set of equispaced perturbations to establish an

approximate location of the ellipsoid's major axis. Next, based on this estimated major axis a new set of coordinates which are constrained to the caps of the 20° spherical double cone centered on this axis is generated. After the completion of the dynamically generated perturbations, the stiffness ellipsoid is recalculated and a final set of coordinates constrained to the plane of the major axis are executed to more thoroughly sample the space containing the minor axes.

We found that this iterative technique did yield improved results. This was especially apparent when considering the shift in the calculated ellipsoid between the first and second stages of the algorithm; the polar sampling appears to provide the extra sampling needed to accurately determine the orientation of the stiffness ellipsoid.

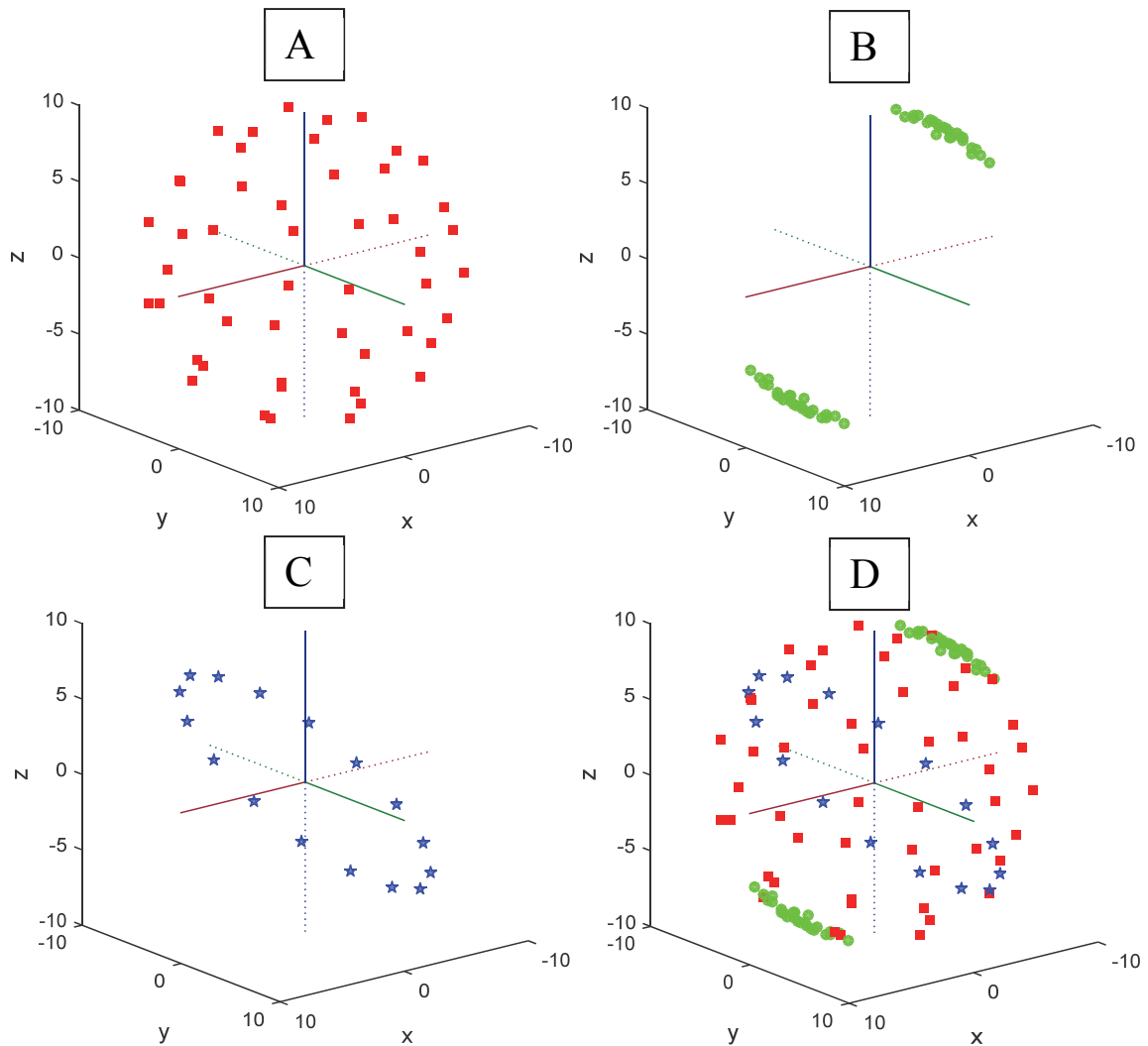


Figure 3.5 The first phase of the dynamic major axis search uses even distributed perturbation directions (A) to get an initial set of force responses. A stiffness ellipsoid is calculated from these perturbations and a new set of perturbations (B) is generated clustered around the major axis of the ellipsoid. The stiffness ellipsoid is recalculated to include the new data and a third set of perturbations (C) is generated in the plane of the major axis which improves the sample density at the minor axes. The overall set of perturbation directions (D) samples densely in the regions where the responses change the most rapidly and sparsely where the curvature is less pronounced.

While the dynamic major axis search method was selected as the main technique for this study, the intermediate calculations to determine the stiffness ellipsoids and

generate new coordinates were performed in MATLAB which required a higher level of user interactivity than one would expect in a commercial product. Initially, the entire collection process required approximately 5 minutes per trial; however, with improved operator training this time was reduced to 3 minutes. However, if we used the equispaced technique with the same resolution as in the second stage of the dynamic method each trial would require over 1000 perturbations taking nearly 19 minutes to complete.

3.2.4 Data Processing and Analysis

Each trial yields an extremely large set of raw data from multiple sources and it's not possible to distill all the information gathered into a single meaningful graphical representation. Thus, we created a suite of analysis techniques that can be used to highlight and examine different aspects of the dataset. Furthermore, as most means of contemporary scientific communication rely on static 2d figures, we needed to devise ways to translate our 3d results into this format.

3.2.4.1 Map Projection

One of the biggest challenges in visualizing each dataset is that each data point consists of 2 3d vectors. Were these vectors 2d, the accepted method of plotting is the vector field. Due to radial sampling paradigm, our perturbation vector in spherical coordinates can be reduced to a 2D vector since the radius component is the same for every sample. We can thus use a map projection to flatten this vector space into a 2D area with the azimuth and elevation angles as our axes.

Unfortunately, this technique cannot be applied to the force vector as there is no trivial components that can be eliminated. This prevents us from creating a proper vector

field as there is no way to represent our forces with a single 2D vector. It is possible to use multiple 2D vectors to fully describe the actual force, but these plots are extremely non-intuitive and hinder the visualization of the data. We found that simplifying the force response to the scalar magnitude was a good compromise and used a color scale to represent the force generated at each perturbation direction.

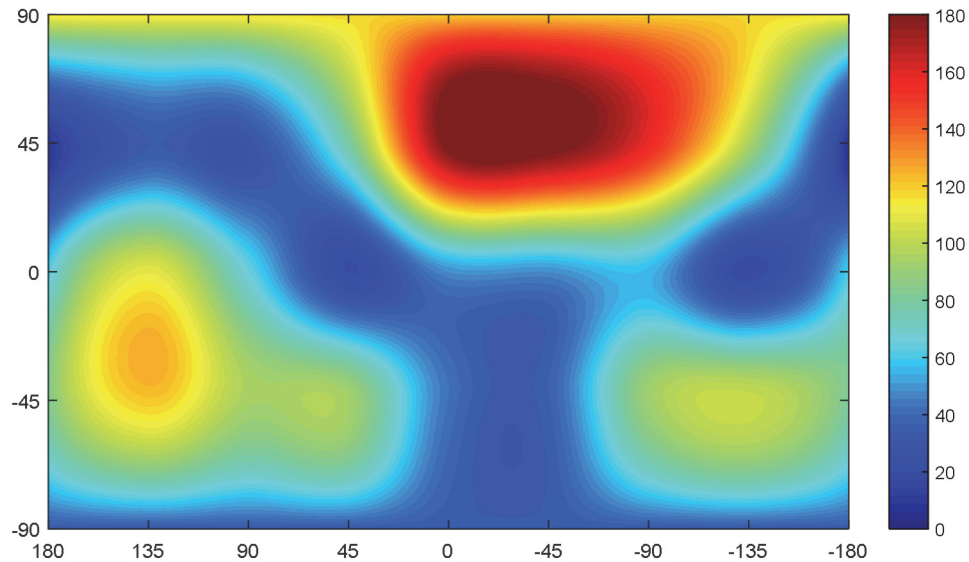


Figure 3.6 Using the clockface and rotate sampling pattern, force magnitudes can be mapped onto a 2D projection. The color scale indicates normalized scalar magnitude at the coordinates indicated by azimuth on the horizontal axis and elevation on the vertical. While this allows the easy visualization of the measured space, force directionality is not preserved.

This method makes it easy to visualize the perturbation space and identify which directions cause the greatest force response. However, the loss of directionality information prevents us from drawing proper conclusions about limb stiffness. Furthermore, this technique suffers from the same distortion issues faced in cartography where the plot becomes exaggerated towards the poles. For our purposes, the area on the

graph is not particularly meaningful so we did not make any attempt to mitigate this distortion.

3.2.4.2 Stiffness Matrix

In order to examine the relationship between perturbation direction and response force direction we calculate the stiffness matrix. In a single dimension the relationship between response force (F) and displacement from resting position (d) is proportional with a stiffness constant (k) and can be described by the following equation:

$$F = k \cdot d$$

In higher dimensions, we must take into account the interactions of each component of force and displacement individually resulting in the following relationship:

$$\begin{bmatrix} F_x \\ F_y \\ F_z \end{bmatrix} = \begin{bmatrix} k_{xx} & k_{xy} & k_{xz} \\ k_{yx} & k_{yy} & k_{yz} \\ k_{zx} & k_{zy} & k_{zz} \end{bmatrix} \times \begin{bmatrix} d_x \\ d_y \\ d_z \end{bmatrix}$$

Each term of the matrix, k_{ij} , represents the stiffness that describes the force that produced in the i direction due to displacement in the j direction. Despite the increased dimensionality, this model is simply a linear relationship between force and displacement allowing us to computationally solve for k using the MATLAB function `mldivide` (backslash operator.) This function uses QR decomposition to find the least squares solution to the system of equations derived from each perturbation.

In an ideal and purely mechanical spring-like system the proportional relationship defined by Hooke's law would hold true. However, we found that in the decerebrate cat hindlimb that the force responses were not symmetric around the origin and were biased towards the proximal direction. This bias is possibly due to muscles not being fully loaded or developing tone throughout the perturbation. Even real springs have a limited

operating range beyond which they do not follow Hooke's law and a system of springs can be constructed where not all elements remain in their operating range over the displacement range of the entire system. The result would be analogous to our findings on the cat hindlimb where the system stiffness is not symmetric about the origin.

Due to this non-spring-like behavior, Hooke's law was an imperfect fit to our data and when graphed as an ellipsoid centered at the origin clearly did not match the physical system. Based on our assumption that this was due to muscles being shortened outside of their operational range, the obvious correction is a piecewise set of Hooke's law equations to account for the discontinuities. However, this model would have required data on the loading of every muscle in the limb and increased sampling to ensure sufficient data points for each section of the piecewise space. Both requirements are in direction opposition of our goals of describing the mechanics of the limb without studying individual muscles and minimizing the duration of sampling.

Instead, we took a simpler approach of simply accounting for the apparent offset with by adding a constant to the equation:

$$\begin{bmatrix} F_x \\ F_y \\ F_z \end{bmatrix} = \begin{bmatrix} k_{xx} & k_{xy} & k_{xz} \\ k_{yx} & k_{yy} & k_{yz} \\ k_{zx} & k_{zy} & k_{zz} \end{bmatrix} \times \begin{bmatrix} d_x \\ d_y \\ d_z \end{bmatrix} + \begin{bmatrix} c_x \\ c_y \\ c_z \end{bmatrix}$$

The force centroid c encapsulates the net effect of any discontinuous behavior of the individual muscles. While this simplification slightly diminishes the mechanistic interpretation of the model, it greatly improves the accuracy without introducing excessive complexity. An alternative interpretation of the force centroid c is that the cat nervous system is actively producing this force bias regardless of the direction of perturbation. While a reason for this is not entirely obvious, this explanation is essentially

what we described with our model and cannot be entirely dismissed based on our findings.

Using the non-centered Hooke's law equation, we can solve for the stiffness matrix k and centroid c over the entire duration of the perturbations. We can then plot each element of k and c over time to inspect how the entire matrix is behaving.

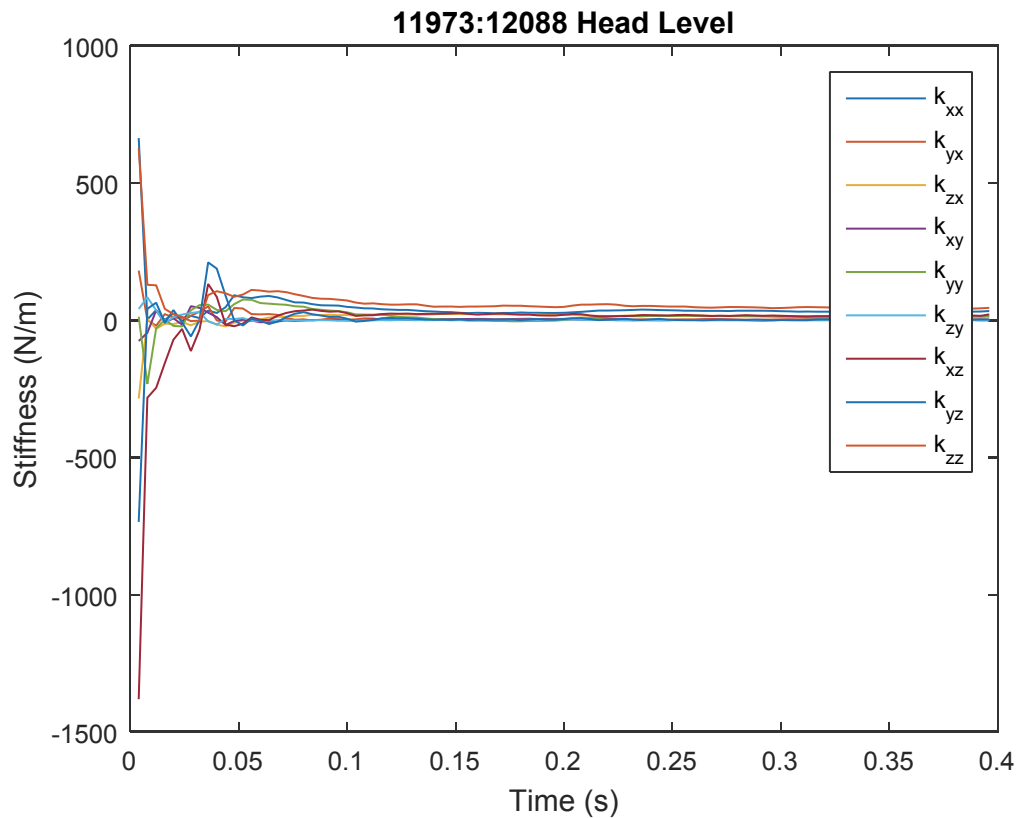


Figure 3.7 The stiffness matrix is calculated at sample over the time course and each element is plotted individually. The stiffness matrix fluctuates significantly at the start of the perturbation (0-100 ms) but settles near the end of the movement and through the hold phase. The centroid can also be plotted in this fashion using a y-axis with units of force.

We can see in Figure 3.7 that the stiffness matrix typically settles to stable values once the perturbation reaches the hold phase at 100 ms. Furthermore, we usually found that the stiffness matrix was approximately symmetric, i.e. that $k_{xy} \approx k_{yx}$ and so forth. If the limb

were behaving like a system of ideal springs, we expect the stiffness matrix to be perfectly symmetric. However, when these pairs of terms deviate, it is possibly an indication of neural patterns modifying the basic spring-like nature of the limb.

3.2.4.3 Projected Ellipsoid

While plotting the stiffness matrix can allow us to perform a deep analysis of each component of the limb stiffness, it is not well suited to visualize the limb response as a whole. When analyzing a 2D stiffness matrix, it is common practice to multiply the matrix by a unit circle to yield a stiffness ellipse. In this vein, we multiplied our 3D stiffness matrices by a unit sphere to give us a stiffness ellipsoid.

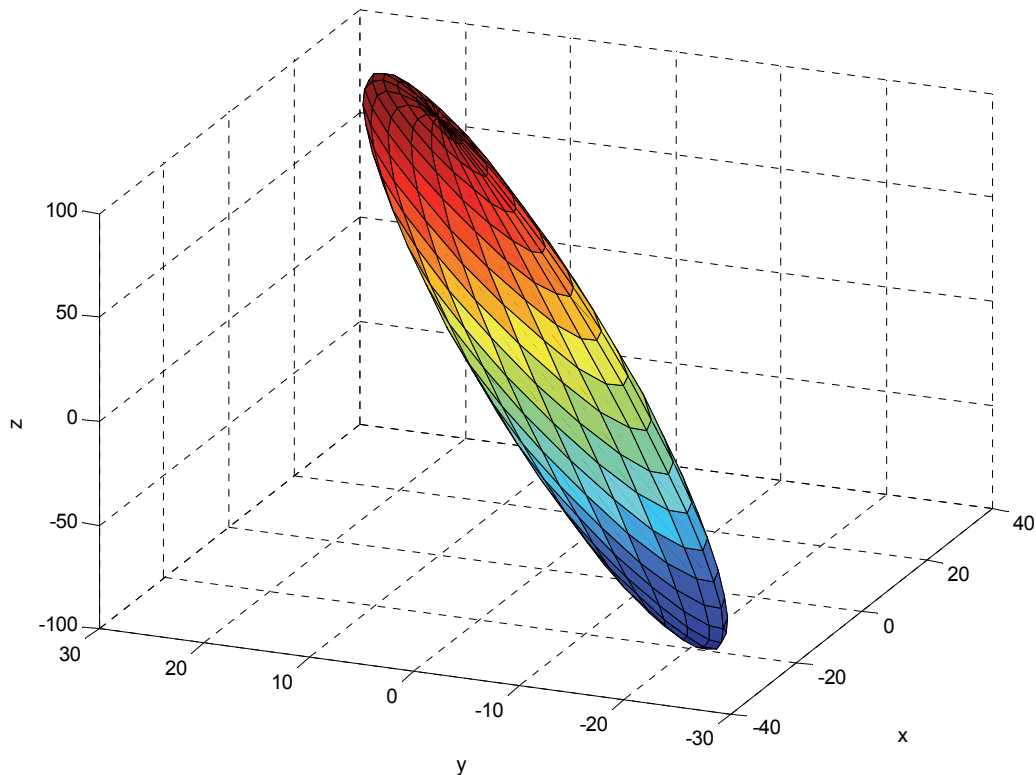


Figure 3.8 The stiffness ellipsoid is visualized by multiplying the stiffness matrix k by a unit sphere. Scaling by the length of the perturbations gives a force ellipsoid which corresponds to a geometric fit

of the measured forces. The color scale indicates vertical component of stiffness and is included for the purpose of improving the visualization of the ellipsoid shape.

Since the perturbations that we used in this study were all of a constant radius, this ellipsoid additionally serves as a representation of the actual force responses if we make the unit sphere the size of the perturbations. In this format, it is easier to visualize the geometric changes that are contained within the stiffness matrix.

We can further simplify the stiffness ellipsoid and make it graphically suitable for conventional media by projecting it onto 2D planes. We found that a sagittal and horizontal projection best capture the critical aspects of the stiffness ellipsoid.

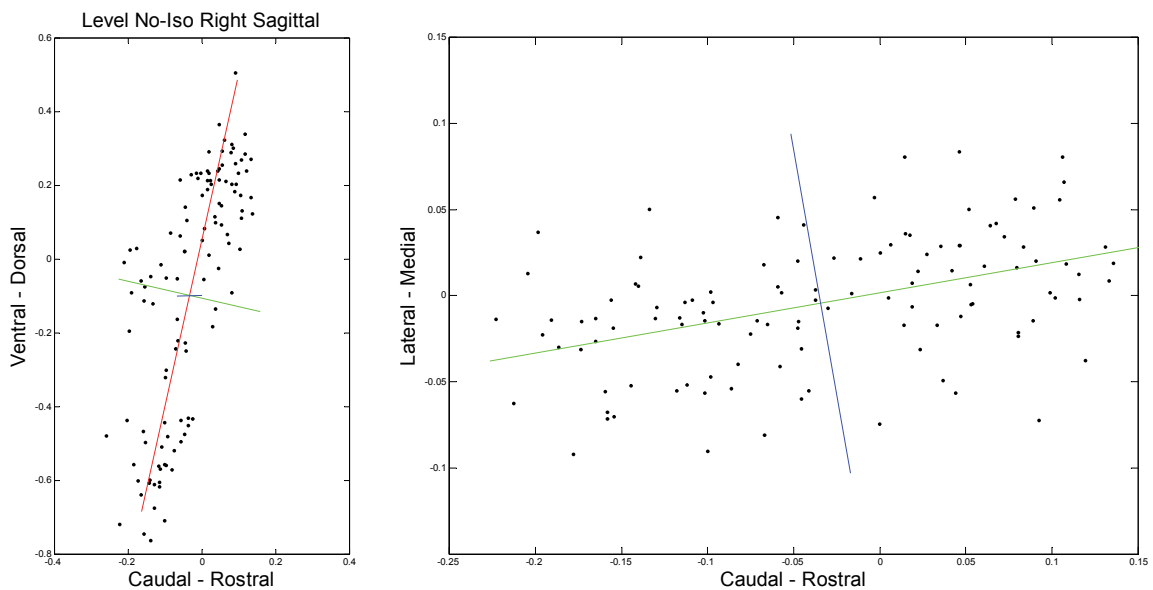


Figure 3.9 By projecting the cloud of force responses onto the anatomical planes allows for easier visualization in 2D. This also facilitates comparisons with results from studies that were performed in 2D.

Furthermore, this allows for easier comparison to other studies which only performed perturbation in the horizontal and sagittal planes.

3.2.4.4 EMG Map

The raw EMG data was bandpass filtered from 40 Hz – 600 Hz to eliminate any DC offset and movement artifact. A 60 Hz notch filter was also necessary to eliminate electrical mains noise. The EMG response was calculated by subtracting the rms magnitude prior to the perturbation from the rms magnitude after the end of the robot movement.

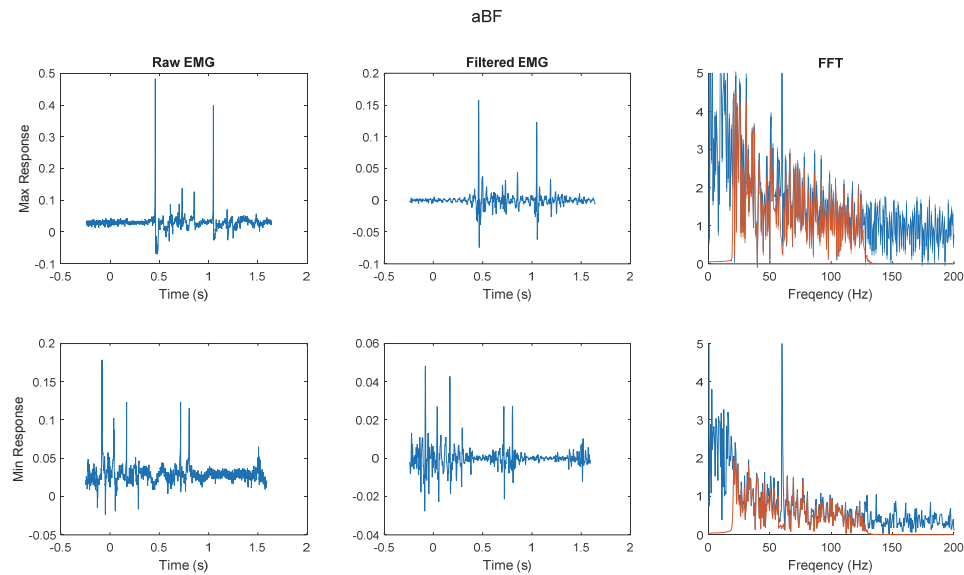
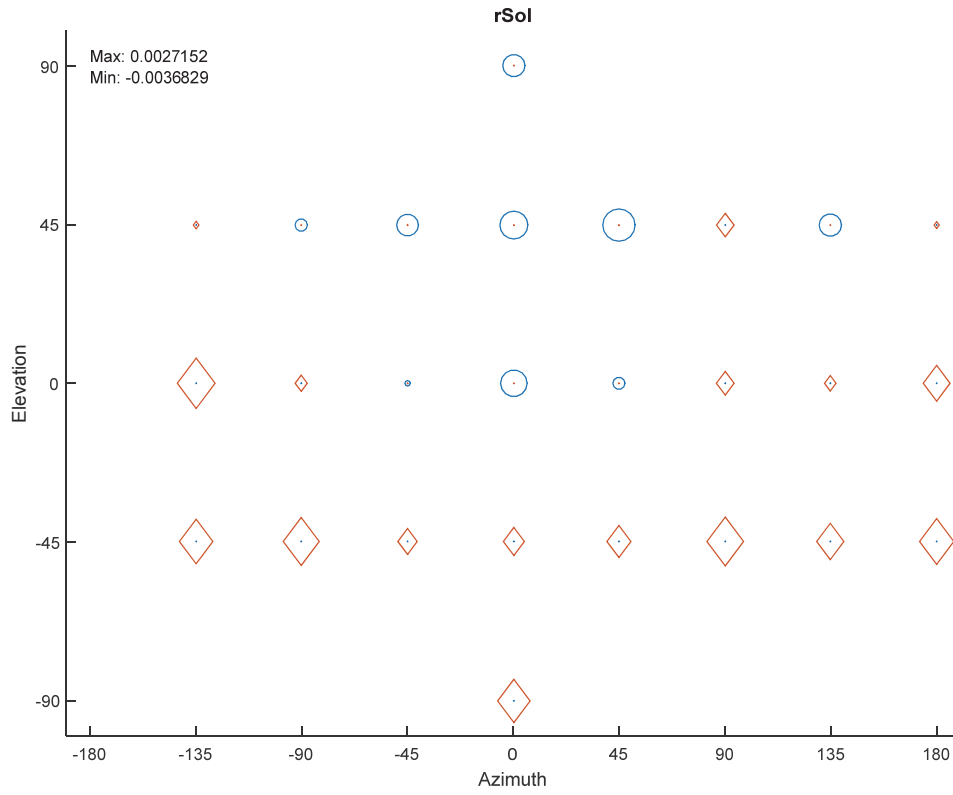


Figure 3.10 Raw EMG contained substantial movement artifacts and mains noise. The top row of plots taken from the largest response of aBF and the bottom row is the minimum response from the same trial. The EMG is filtered with both a bandpass filter and a 60 Hz notch filter allowing muscle activity to be isolated. In these examples the bandpass filter was set to 20-125 Hz to better illustrate the filter performance at the cutoff frequencies.

In order to visualize the spatial nature of EMG responses we used the same mapping technique as described in 3.2.4.1. At each sampled location, we plotted an open circle marker the area of which represents the EMG response normalized to the largest response. Due to the fact that it was possible that some perturbations could cause a

reduction in activity for some muscles, we had to account for negative valued responses which are indicated by marker color.



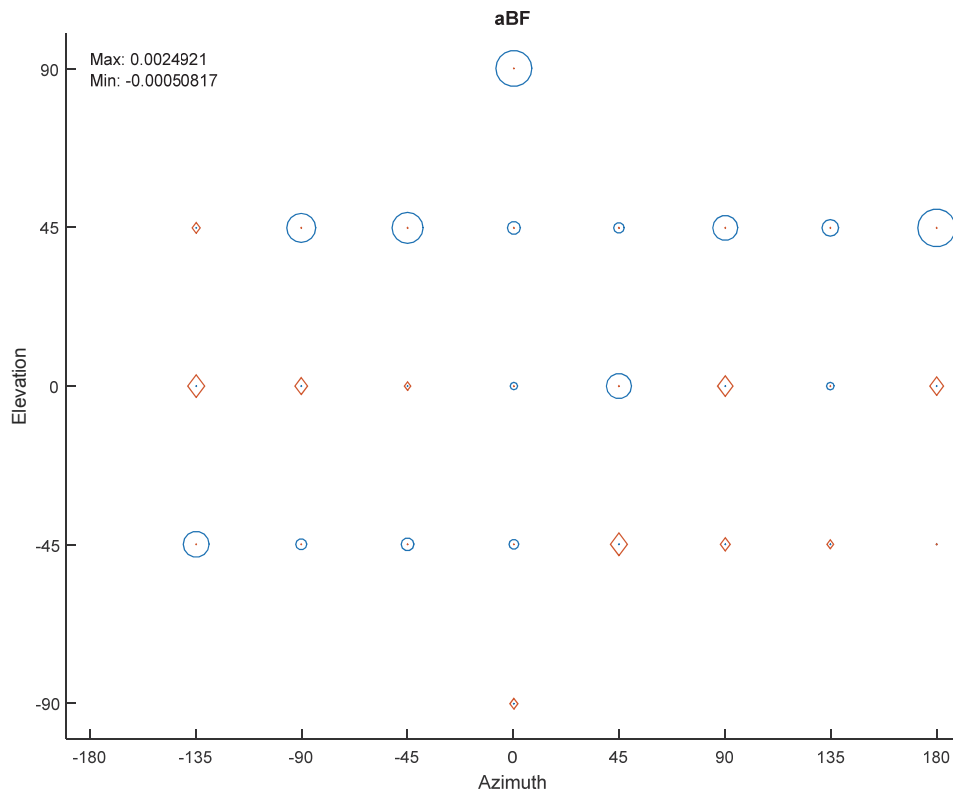


Figure 3.11 EMG can be plotted against perturbation direction with marker size indicating integrated RMS EMG magnitude. The blue circles represent increased EMG activity while the red diamonds denote a reduction in EMG activity as compared to baseline.

It is important to note that unlike the force response mapping described in 3.2.4.1 the size of the markers is not distorted at the poles. However, due to the necessity of normalizing the marker size to ensure readability, it is necessary to consider this factor when comparing between experiments and between muscles.

3.3 Discussion

While this robotic system did meet the design goal of measuring hindlimb stiffness in the decerebrate cat we found that it was unable to perform well when the cat behaved erratically. Unfortunately, there is very small margin for error for the modified

premamillary brainstem transection even under ideal surgical conditions. Thus, there is an inherent compromise between the desired reactivity and undesired spontaneous activity. Instances in which the decerebrate cats pull their paws off the force sensors are by far the most disruptive as it can result in the removal of EMG electrodes and requires the experimenter to carefully reattach the paw to the robot with the same initial positioning. However, as the decerebrate cat cannot process pain signals it is highly probable that a stronger fixation at the foot would result in injury to the animal. Consequently, due to the lack of repeatability of highly reactive decerebrate cats, the most reliable stiffness measurements were only able to be made at low forces.

While we designed and tested this robotic system for the use with decerebrate cats it is possibly better suited for use with human subjects or trained animals. We expect that with the addition of hand grips to the force/torque sensors that this system can be immediately adapted to make stiffness measurements with the human arm. Furthermore, due to the modular design of this system the robotic arms and force sensors can be replaced with models capable of larger maximum loads which would allow the system to be used with human legs. Additionally, trained animals and humans would generally not need a support frame to and thus there would be less interference with the capture of kinematic data. Furthermore, the removal of the support frame would allow for greater spatial freedom of the robots and would enable the testing of a wider range of initial limb position.

Our robotic system can also be easily configured to perform 2D planar perturbations. The ability to compare and reproduce results from earlier studies is important as it allows for some comparison between the systems and a level of validation

for the techniques. Honeycutt and Nichols (2010) used our robotic system to record horizontal plane tuning curves of decerebrate cats with LG/Sol reinnervations after the original planar robot had been decommissioned. While the perturbation profiles were identical to the original apparatus, our arm-based robotic system allowed for much shorter inter-sample intervals resulting in a greatly reduced collection time. The rapid collection of data greatly reduced the chances of sporadic decerebrate cat movements from affecting a run. Furthermore, the shorter collections help to mitigate the changes in limb response due to the long-term deterioration of the decerebrate cat.

Our system was also successfully employed by Martin (2013) to record the 2D stiffness properties of the decerebrate cat forelimb in the sagittal plane. The only additional equipment that was required for these experiments were scapula clamps as the external hip clamp was inadequate to stabilize the shoulder. Measurements were constrained to the sagittal plane as the primary objective of these trials was to provide a comparison to the results of a mathematical model; however, a full 3D measurement of forelimb stiffness could be made using the same setup. This use case demonstrates the value provided by our robotic system as it can be easily reconfigured for different experimental paradigms with minimal additional cost.

While 1D recordings on the decerebrate cat hindlimb were initially performed as a diagnostic during the development of the robotic system we found that this technique to be valuable to measure stiffness changes during conditions with variable background force such as XER. Despite the ability to perform linear perturbations around any arbitrary axis, the loss of dimensionality prevents any definitive analysis of the spatial nature of the limb stiffness. In practice, the single axis perturbations are also susceptible

to paw-off events when taking measurements on the decerebrate cat and using XER inherently limits collection from only one leg at a time due to the accompanying withdraw response on the stimulated limb. However, with an alternate limb fixation isolating a single joint rather than allowing the entire leg to move freely small linear perturbations could be used to measure stiffness of that individual joint.

Another potential feature that we have permitted by our framework is the ability to move the robotic arm based on closed-loop feedback from the force/torque sensor. This could allow for the simulation of various real-world scenarios such as interacting with an elastic spring or moving through a viscous environment. Additionally, this could be used to apply programmed force perturbations rather than the displacement-oriented perturbations that were used in this project. From a safety perspective, it would be necessary to implement a means to detect when the subject is not in contact with the force sensor to prevent aberrant movements if suddenly unloaded.

One drawback to our current method of performing the dynamic major axis search is that the stiffness calculation phases are performed on the data collection computer and require the user to manually execute the updated perturbation set. Despite having streamlined this process, the technique could be improved by performing the stiffness calculations directly on the robot controller. If the stiffness was recalculated between each perturbation it would be possible to automatically determine when enough samples have been collected for the matrix to converge on a stable measurement of stiffness. While this would introduce a slight delay between each individual perturbation as the robot controller's computing power is very low by modern standards, the benefit of minimizing the total number of perturbations is a valuable trade-off, especially for

measurements on animals or patients who cannot endure lengthy collections. Ideally, a robotic system would be capable of performing a continuous, dynamic collection and calculation of stiffness data. Unfortunately, the current version of the robot controller hardware simply does not have the computing capacity to execute all these functions simultaneously. However, as the computational difficulty of these tasks is effectively capped by the fact that we are limited to 3 physical dimensions, future versions of the robot hardware will eventually be capable of continuous, real-time measurements of stiffness.

Overall, the modular nature of our system is the greatest feature of this system as it enables a much greater range of scientific and clinical applications than prior systems that were designed for a singular task. Not only does using an industrial robotic arm lower equipment cost due to market competition, they are designed to have long service lives and support cycles from the manufacturer which could result in lower long-term maintenance costs. As the modular design provides the possibility of upgrading and customizing individual components as the users' requirements grow and change we expect our system to be a very cost-effective solution for anyone needed to make biomechanical measurements.

CHAPTER 4

FELINE HINDLIMB STIFFNESS

4.1 Introduction

Based on our finding that the feline modulates muscular reflexes in response to altered support slope angle it follows that net endpoint stiffness of the cat limbs are likewise altered to meet the demands of the specific task. On a sloped surface, locomotion tasks must account for a portion of gravitational force opposing or assisting forward movement. Additionally, the portion of gravity normal to the sloped surface results in reduced friction between the paws and ground which could require additional effort to maintain grip.

Furthermore, both locomotion and standing tasks can only be successful when the center of mass of the animal remains over the base of support. The maintenance of balance on a sloped surface can be achieved in multiple ways. Increasing the area of support can mitigate the relative shift of the center of mass. Likewise, adopting a crouched posture will slightly shift the center of mass towards the center of the support base. Finally, the cat could lean in the upslope direction to reposition the center of mass. In the quadruped, there is a large tolerance margin due to the support area being nearly the entire body length. Even though modifying posture is not strictly necessary on modest inclines allowing the center of gravity to approach the edge of the support area makes the animal more susceptible to falling if perturbed. Since the base of support of bipedal animals is much smaller relative to body size the modulation of posture based on slope angle is even more critical for successful standing and locomotion than in our quadrupedal model.

The endpoint stiffness of the limb encapsulates any number of different strategies that the cat may use to maintain balance or gait on a sloped surface as it measures the net force produced by the cat as well as accounts for passive limb mechanics. Using the robots developed for this project we were able to make 3D measurements of hindlimb stiffness and study how this stiffness was modulated by the body orientation signal. Based on our finding that intermuscular inhibition between some hindlimb muscles was increased in the downslope condition we hypothesized that we would find a corresponding decrease in limb stiffness under the same head tilt state.

While the modulation of intermuscular reflexes was less consistent in the upslope condition it is possible that our limited combination of intermuscular interactions measured failed to capture the primary modulation targets. Thus, we expected that when measuring the whole limb stiffness that we would find increased stiffness in the upslope condition resulting in a continuous trend over the whole range of slope angles.

4.2 Methods

4.2.1 Surgical Preparation

20 female cats were used in this portion of the study including those which were used in combination with muscle puller experiments. These methods were approved by the IACUC of Georgia Institute of Technology. Each cat was initially anesthetized in an induction chamber using 5% isoflurane mixed into a 95%/5% blend of O₂ and CO₂. Anesthesia was verified by a lack of withdrawal reflex and muscle tone. The cat was then transferred to a surgical table and isoflurane administration was switched to a mask. Finally, a tracheotomy was performed to ensure a consistent airway for the duration of

the experiment. Isoflurane was used as the sole anesthetic agent due to the short duration of lingering effects once anesthesia is removed.

Using the same window created for the tracheotomy the external jugular vein is cannulated for the intravenous administration of fluids. Both carotid arteries are loosely ligated in advance of the decerebration procedure so that they can be quickly tied if there is excessive cranial bleeding. A bilateral labyrinthectomy was performed by exposing the auditory bullae with blunt dissection and then piercing each with a sharp probe and destroying the vestibular labyrinths. This procedure had the potential to disrupt the internal vasculature and cause minor bleeding; in these cases, a small amount of gauze was packed into the bulla and held with pressure until hemostasis was achieved.

4.2.2 EMG Electrode Implantation

Prior to decerebration EMG electrodes were implanted into various hindlimb muscles. During early experiments fine, stranded stainless steel wire electrodes were sutured into individual muscles with care taken to minimize the number of skin incisions. We were able to access all muscles of interest with 3 incisions per leg: on the lateral-dorsal/posterior shank, lateral mid-thigh, and medial proximal thigh. The incisions were closed with stainless steel wound clips with care taken to ensure that the electrode leads remain free. Unfortunately, using this method left the electrodes susceptible to movement artifact from the robotic perturbations. We determined that this was caused by the inertia of the electrode leads causing small movements at the point of electrical contact. Securing the electrode leads to the skin near the incision provided some strain relief and reduced the magnitude of the artifacts but did not completely eliminate them. Additionally, we found that in some preparations erratic movements resulted in the

electrode leads becoming caught on the cat's leg and subsequently pulled from the muscle. On highly active and responsive preparations such as these, it was infeasible to attempt to reimplant the electrodes and thus the EMG records from the affected muscles could not be obtained.

To solve both the problems of electrode strain relief and accidental removal, we routed the EMG electrodes subcutaneously so that they exited on the back. This technique provided the most reliable EMG signal as the large contact area between the leads and the skin almost completely prevented movement at the insertion site. Using this technique, we had no instances of electrodes becoming accidentally removed due to unexpected movements. However, there is no exit location on the body that is completely protected; as such, a wireless telemetry system which could remain entirely implanted is the ideal solution to protect EMG electrodes.

While subdermal routing improved signal fidelity, it came at the cost of additional time that the cats remained under anesthesia. It is ideal to minimize the time under anesthesia to maintain the health of the preparation and reduce the possibility of lingering isoflurane affecting the results. Additionally, in the case that an electrode malfunctioned using the surgical method, there was no way to replace it without reanesthetizing the cat and performing the entire procedure again and carried the possibility to disturb the working electrodes. In order to address these limitations, we developed a novel electrode implantation technique using a percutaneous needle introducer.

The new electrodes were built from 20 AWG solid stainless steel wire. The extra rigidity compared to the fine stranded wire normally used was critical to the design. This wire was threaded into an 18 gauge hypodermic needle and the tip of the wire exiting the

sharp of the needle was stripped and bent into a barb. This served as the electrical contact surface of the electrode as well as the anchoring mechanism. Prior to deployment, the electrode wire was retracted into the needle such that only the barb was exposed.

An experienced investigator was able to deploy these electrodes percutaneously by puncturing through the skin and into the target muscle. Once the needle was inserted to the desired depth it was retracted allowing the electrode to remain in the muscle. Alternatively, the target muscles were visualized prior to implantation using extremely small incisions in the skin. The needle was retained on the electrode lead and was secured with tape to prevent accidental needle sticks. Using this implantation method reduced the amount of time the cats were under anesthesia by over an hour and was less disruptive to the skin and fascia. Furthermore, the electrodes can be quickly refurbished by cutting off the end and making a new barbed contact allowing for additional time savings over traditional fine wire electrodes when reimplantation was necessary. While reinstallation or addition of new electrodes after the withdraw of anesthesia was not necessary in any of our experiments, this technique should allow the experimenter to perform this task if needed.

The time savings from the percutaneous electrode installation technique came with some tradeoffs as compared to subcutaneously routed fine wire electrodes. The motion artifacts that were almost entirely eliminated by subdermal routing were occasionally present using this method. However, the magnitude and incidence of these artifacts were lower as compared to the conventional fine wire technique. This is possibly due to the electrode being anchored at the precise point of electrical contact reducing the movement at the electrical interface.

While the insertion of the electrodes was considerably less invasive and potentially damaging to the tissue as compared to fine wire electrodes which were sewn into the muscle, the reduced flexibility of the wire had the potential to damage the muscle over the duration of the experiment. Post-mortem inspection of electrode implantation sites showed no visible indication of damage such as discoloration, bruising, or tearing. However, the risk of tissue damage caused by forceful removal of the electrodes is high and as such, this design is only appropriate for terminal procedures in restrained limbs which have a lower chance of accidental removal.

In experiments that used XER to modulate the background limb force, a cuff electrode was implanted on the tibial nerve(s) contralateral to the limb being measured. The electrode cable was taped securely to the skin to prevent accidental removal. It was sometimes necessary to clamp the contralateral foot to counteract the withdraw reflex and prevent interference with the limb being measured.

4.2.3 Decerebration

Once all implantations were completed, the cat was transferred to a stereotaxic frame. This portion of the study made use of the modified premammillary decerebration and brainstem transection developed by Honeycutt (2009) for a similar planar robotic manipulator. This technique yields a preparation that is highly reactive to sensory input but does not exhibit stepping. The initial craniotomy was performed with a manual trephine and rongeurs. Bone wax was applied to the remaining edges of the skull to prevent bleeding or air emboli. Excessive bleeding was also curtailed by ligating the carotid arteries. The cerebral cortices were resected, and the brainstem was exposed. Using the cerebellar tentorium as a reference the brainstem was transected at a 45° angle,

the same technique as a standard premammillary preparation which would result in a spontaneously locomoting preparation. A second vertical transection was then performed rostral of the tentorium near the subthalamic nucleus.

The second transection disrupts the pathway that initiates stepping, but preserves the ability to respond to postural perturbations (Honeycutt 2009). During some experiments, spontaneous locomotion was present despite the second transection and a third transection was performed slightly caudal to the second. It was important for the reattempted transection to be as near as possible to the original location and as sharp an instrument as possible, such as a fresh scalpel, was required. Various hemostatic agents including Gelfoam, QuikClot, thrombin, and cotton were packed into the cranium and the isoflurane concentration was gradually reduced to 0% over 30 minutes. If there were no signs of bleeding once anesthesia was removed, carotid circulation was restored.

In one experiment, an intrathecal catheter was inserted for the administration of 2,5-Dimethoxy-4-iodoamphetamine (DOI). The lower thoracic vertebrae were exposed and all soft tissue was resected. Under isoflurane anesthesia, a dorsal laminectomy was performed exposing the spinal cord. Light traction was applied to the meninges so that a small incision could be made without contacting the spinal cord. A thin flexible catheter was threaded into the intrathecal space. The catheter was secured to the skin to maintain its position and prevent potential damage to the spinal cord. The wound was temporarily closed with alligator clips so that placement could be verified during DOI administration and to minimize fluid loss in the interim.

4.2.4 Mechanical Support

In addition to the stereotaxic head fixation and a sling supporting the trunk, external supports were used to secure the hindlimbs. The base of the tail was shaved, wrapped with tape, and clamped at a height at which the trunk of the cat was roughly horizontal. The head and tail supports were sufficient to support the entire weight of the cat, but the sling was used to distribute the weight more evenly and compensate for the reduced tone caused by anesthesia and decerebration. Additionally, the tail clamp was sufficient to counter the force of the robotic perturbations below the horizontal plane. However, the tail clamp was not able to prevent motion in the lateral or dorsal directions. To prevent the hips from moving during these perturbations, an additional clamp was affixed above the sacrum that extended ventrally around the pelvis. Conventional hip pins were not employed as it has been previously observed that hindlimb activity is greatly suppressed when used. While the specific mechanism of this suppression has not been identified, the compression of tissues between the pins and skeleton is the most reasonable cause. Our hip clamp, made from a modified Irwin QUICK-GRIP Handi-Clamp, was specifically designed to have a wide area of contact and minimize the pressure on the skin while preventing dorsal and lateral movement of the hip joint.

4.2.5 Robotic System Integration

The paws of the hindlimb were attached to the force sensor of the robotic manipulator using adhesive tape. To maximize adhesion, the fur between and surrounding the digital pads was trimmed. Double sided carpet tape was preferred as it employs a strong adhesive, was easy to apply, and did not require curing. However, during some experiments tape alone was insufficient to keep the paw attached to the

robot. In these cases, cyanoacrylate glue was used to bond the toe pads to the tape surface. The interface between the tape and force sensor was maintained under all conditions due to the much larger contact area as compared to the paw. While the glue provided a much stronger adhesion than tape alone and had a very rapid curing time of about 10 seconds we did not use it as our primary technique because we wanted to minimize potential skin irritation. Furthermore, fully cured cyanoacrylate is very rigid and has the undesired effect of locking the skin of the toe pads into a static form. This mechanically inhibits cutaneous sensory receptors and was contrary to our desire to keep the hindlimb sensorimotor system as intact as possible.

The initial location of the paw was set at the height of the treadmill approximately 2 cm posterior to the hip. This was similar to how the legs would be positioned in during the mid-late stance of the step cycle. It was not possible to set the leg in a more neutral, standing configuration due to the risk of collision between the robotic arms and the treadmill support frame. As the initial position of the leg can have a significant impact on the endpoint stiffness of the leg, care was taken to ensure that the foot position was consistent between experiments.

During early experiments, kinematic markers (adhesive-backed retroreflective spheres) were placed on the skin with the intention to record the positions of the hindlimb segments during the robotic perturbations using a Vicon MX motion capture system. In addition to having a record of the limb kinematics, these data would have been used in combination with the records of the force and torque at the paw to calculate individual joint torques and stiffnesses using inverse dynamics. This additional information had the potential to localize the sources of changes caused by altered neck angle.

While the Vicon motion capture system had been previously used successfully with locomoting cats (Stahl and Nichols 2014), we encountered numerous difficulties in collecting complete and accurate measurements and we ultimately decided not to pursue the limb kinematics. Despite using the same treadmill frame as Stahl and Nichols (2014) the additional clamps and supports required to keep the leg stable both blocked the line of sight between the markers and cameras and were reflective to the near-infrared light used by the camera system. With a typical set up, interpolation can be used to compensate for brief interruptions to the markers' paths, but for some perturbation directions the markers were blocked for the entire movement preventing any corrective measures. This was especially problematic for perturbations that moved the paw below the plane of the treadmill as entire trials were obscured preventing any interpolation.

4.2.6 Robotic Data Collection

As detailed in Chapter 3, initial experiments used a 4 cm grid pattern of perturbations to measure limb stiffness which eventually evolved into the dynamic major axis search technique using 1 cm perturbations. Control measurements were recorded with the cat on anesthesia in order to demonstrate that head tilt did not have a passive effect on hindlimb stiffness. At least 30 minutes after the removal of anesthesia, recordings of limb stiffness were taken. There was typically a low amount of resting tone in the hindlimb, but reflexive activity could be detected when manually stretching or shortening the limbs. These recordings were of primary interest as the stable baseline force allowed for the most consistent comparison between cats and head positions. Additionally, recordings were performed during periods of cutaneous stimulation in the form of manual scratching by the investigators. This technique increased the baseline

tone in the hindlimbs and in other studies it has been shown to reflexive activity (Honeycutt 2009) and enhance stepping (Stahl 2010) in decerebrate cats. It was very difficult to maintain a consistent level of background tone with this method, but a larger confounding factor was that the cats occasionally responded extremely strongly to the scratching. In many of these cases, the paw would become detached from the force sensor, but even when the paw remained attached the activity of the reaction would completely dominate and no reaction to the robotic perturbations could be found. It was not possible to calculate a meaningful stiffness matrix from these trials.

2 of the experiments which made use of XER to modulate the background force, robotic perturbations were repeatedly applied along the axis of the leg. This axis was chosen based on preliminary results from other cats which showed that the primary axis of the 3d stiffness ellipsoid roughly coincided with the axis of the leg and would thus provide the largest force responses. As detailed in chapter 3, a stiffness matrix could not be reconstructed from these recordings, however different head tilt directions could be compared by examining the differences in the force responses. Alone, these data could not provide a definitive understanding of the changes in the limb mechanics, but using the context provided by the 3D stiffness matrix calculations we were able to use this method to bolster our understanding of the overall effect of head tilt on hindlimb stiffness.

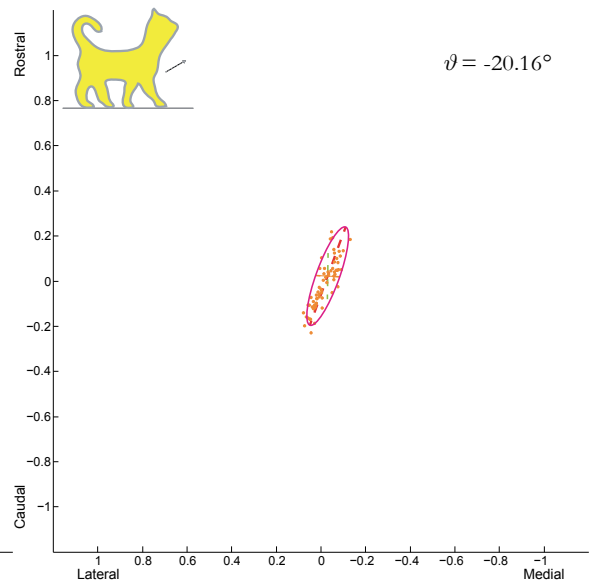
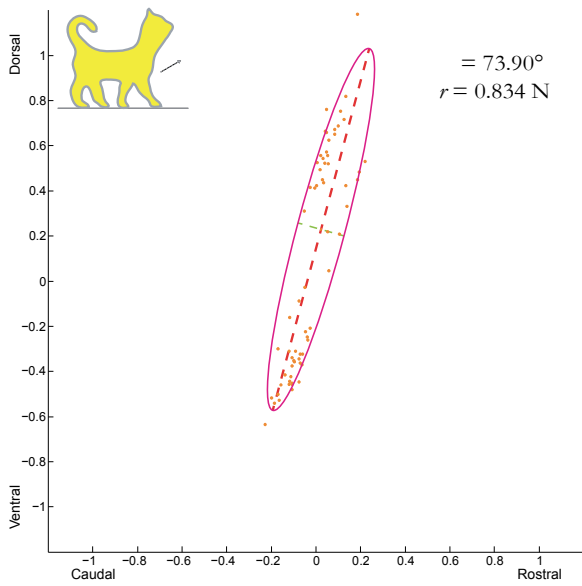
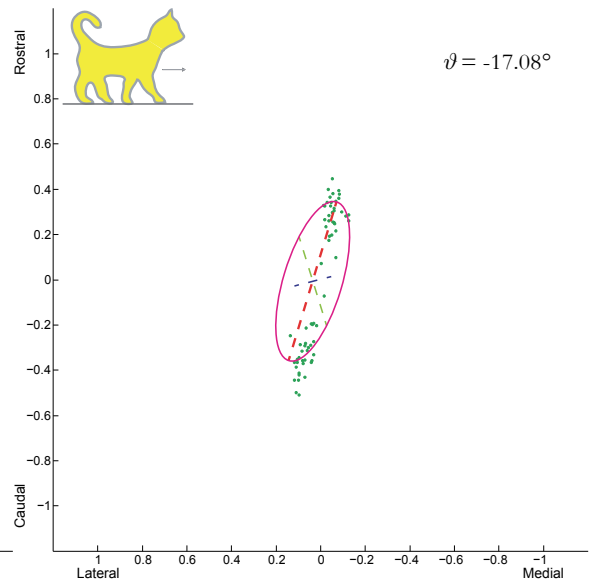
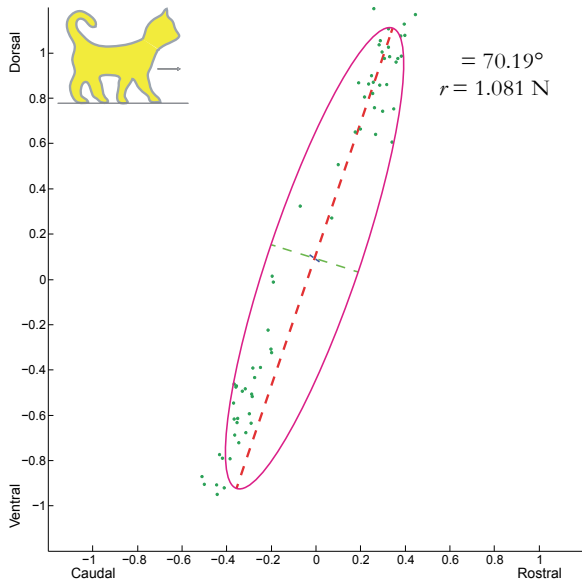
On 4 cats we attempted to collect muscle puller data after a shortened robotic stiffness session. These cats had to be reanesthetized in order to perform the surgical dissection of the shank muscles and implantation of the bone pins. As detailed in chapter 2, a majority of these experiments were unsuccessful as the cats' conditions deteriorated

under anesthesia. However, there was no indication of any problems the robotic stiffness measurements and since the order of the experiments could not be reversed due to the invasive surgery it remains unclear what aspects of the experimental paradigm caused the cats to have poor tolerance to isoflurane anesthesia after robotic experiments.

4.3 Results

Our most reliable results were found during passive conditions where the cat was reactive and off anesthesia, but not actively producing movement generating forces. The baseline force during these trials was very low but was consistent between head positions and across cats. We assume that the baseline force is mostly due to the portion of the legs' weight that was supported by the robotic system instead of the treadmill frame based on the observations that in the absence of the robot, the legs would dangle below the level of the treadmill belt. Furthermore, the legs were nearly flaccid when manually manipulated at low velocities and did not exhibit any clear EMG activity. However, when manipulated rapidly or cutaneous stimulation was applied, muscular activation was clearly observed in increased stiffness and EMG when available indicating that the spinal circuitry was not being suppressed by anesthesia or excessive descending inhibition. We designated this low background force state as "passive" to distinguish it from control trials performed under anesthesia or during active force production. While these passive conditions are not ideal for making inferences about the effect of head tilt on specific motor activities we found it much more important to have a consistent baseline force to ensure that the calculated stiffness accurately reflected a single state of the limb.

In the passive condition, we found that the head-up condition exhibited reduced stiffness as compared to level and head-down trials.



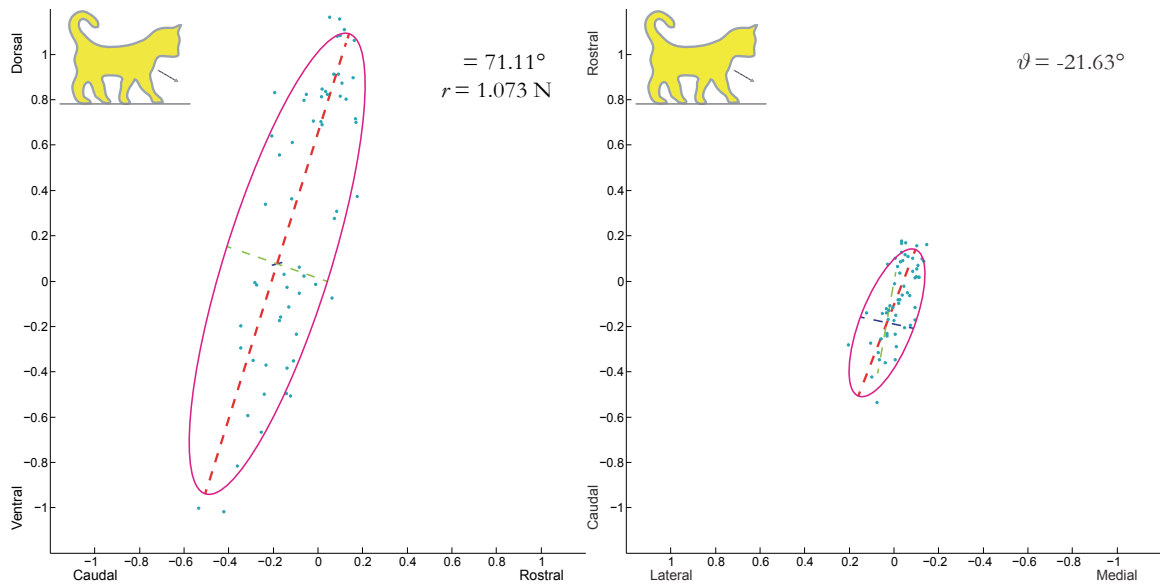


Figure 4.1 Projected passive ellipsoids show reduced overall stiffness in the head up condition. The level and head down ellipsoids have very similar sizes but are oriented slightly differently. While we expected a progressive change between head angles this shows that more complex strategies may be responsible for the alterations needed for sloped task.

In Figure 4.1 we can see that the major axis of the ellipsoid was diminished in the head up condition as compared to those in the level and head up ellipsoids. While the minor axes of the ellipsoid also appear to be smaller in the downslope condition, force magnitude difference between conditions was too small compared to the level of noise in the transducer to have high confidence in those observations. These results agree with our hypothesis and correspond to our earlier findings that showed increased intermuscular inhibition in the downslope condition.

Figure 4.1 also shows a rotation in the ellipsoid in the head down condition as compared to level, but with axis of nearly the same magnitude. While this is representative of the type of change between the level and head down conditions, there was no consistent trend to these differences. Furthermore, similar to the muscle puller experiments 5 cats did not exhibit any quantifiable differences between head positions.

The modified premammillary decerebration used in the robotic experiments did yield a much wider range of apparent activity in the cats as compared to the muscle puller experiments, but this did not seem to correlate with the lack of responsiveness to head tilt.

While the 1D perturbation technique was implemented as a diagnostic tool during the development of the robotic system, the results from those experiments were consistent with the findings from the 3D methods.

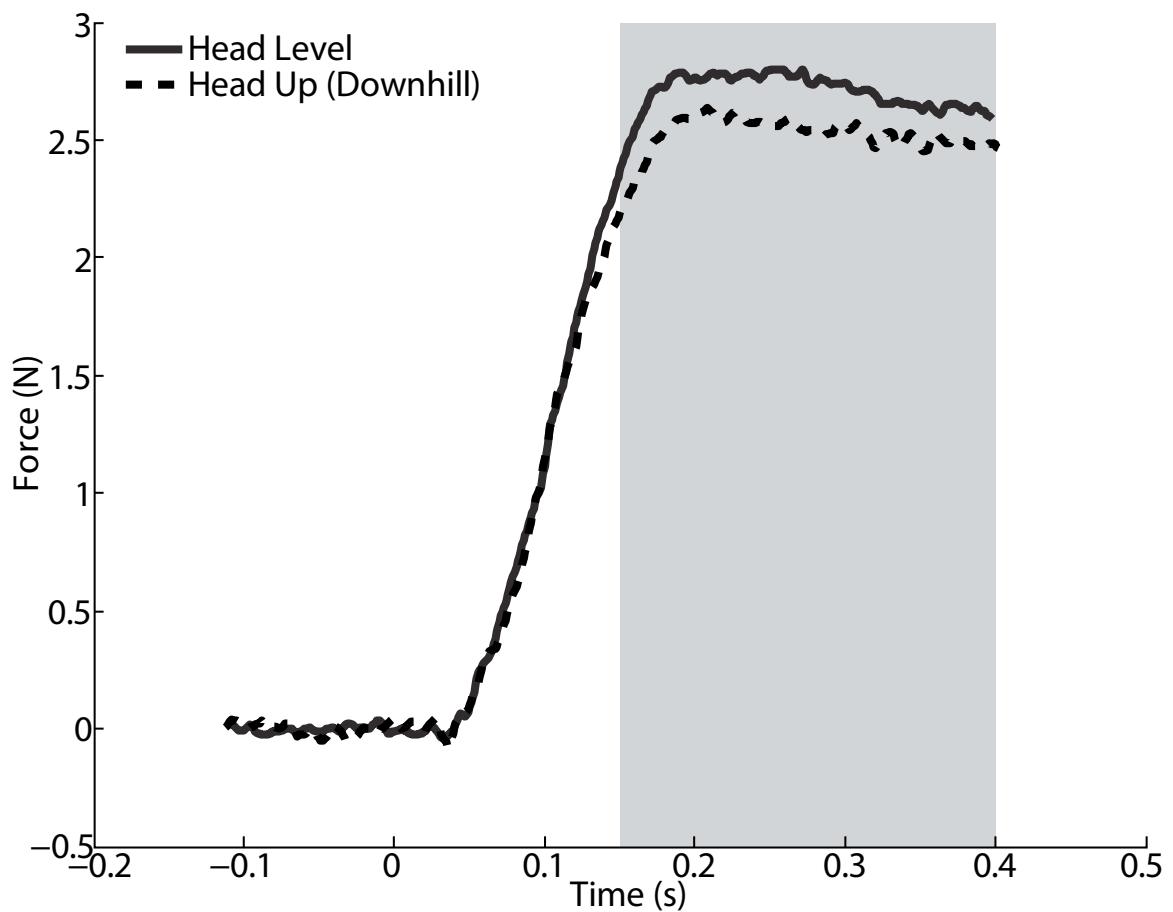


Figure 4.2 Average force responses during XER along a single perturbation axis show reduced force in the downslope case as compared to level and uphill. This matches the trend found with 3D measurements in the passive condition which suggests that the change in apparent force is due to reduced limb stiffness.

Figure 4.2 shows that during XER the magnitude of force responses is significantly lower in the head up condition as compared to level. This appears to be similar to our 3D results which show a reduced stiffness in the downslope condition. While not shown in this figure, the force responses in the head down condition were indistinguishable from the level condition which also corresponds to our 3D results. While we do not have enough observations of this type to make definitive conclusions on their own the similarity to the passive 3D results reinforces the validity of both. Furthermore, this suggests that although the changes with head tilt were most easily detected in the passive condition, they are also present during active motor responses.

Control experiments where robotic perturbations were performed under anesthesia demonstrated that while the passive stiffness ellipsoid maintains a similar orientation to that of an active cat, the magnitude is greatly reduced.

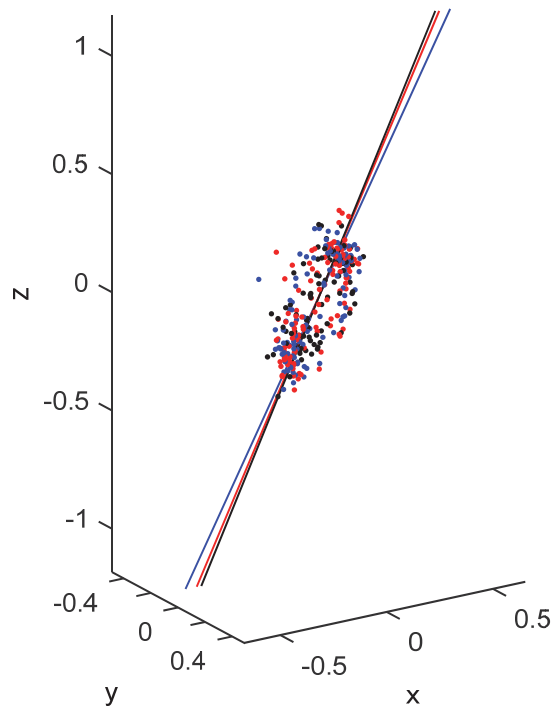


Figure 4.3 Control experiments were performed under isoflurane anesthesia. As expected, all 3 head tilt conditions resulted in nearly identical stiffness ellipsoids. In these trials the limbs were entirely flaccid and the stiffness measured is representative of the purely structural components of the leg. While the force magnitude is significantly lower than those measured in active conditions, the eccentricity and orientation of the ellipsoid is very similar.

Moreover, Figure 4.3 shows that there are no changes between the head tilt conditions under anesthesia. This verifies that our experimental results were not mechanically influenced by the changes to the head pitch. While we did not attempt to determine whether we could intentionally induced changes by altering the center of rotation or rotating beyond 20° , the position of the head tilt motor was assessed for each cat to ensure that the head positions appeared as natural as possible and that the rotation did not produce any visible movement in the torso. We also observed that the eccentricity

and orientation of the control responses was remarkably similar to those measured under active conditions. This was the expected finding as the stiffness pattern in both the active and passive conditions is dominated by the anatomy and positioning of the hindlimb.

Applying cutaneous stimulation around the tail, lower back, and perineum to increase the background force and activity was our least successful methodology. While this strategy had been successfully used with a planar robot (Honeycutt 2009) our longer collection times resulted in data sets that were not internally consistent. While the cutaneous stimulation did result in a more active and reactive state in the cat it did not persist beyond the initial perturbations. Applying the stimulation continuously during the data collection did extend this period of activity in some cats, but none were able to persevere through the entire collection phase. Furthermore, this technique ran the risk of altering the results due to the physical action during vigorous scratching. Finally, the data from these trials showed that force responses clearly showed that the activity induced by cutaneous stimulation overshadowed any response to head tilt or even the perturbations themselves.

As discussed in Chapter 2, we attempted to perform both the robotic and muscle puller protocols on 5 cats. While the goal of these experiments was to bridge our findings between the two techniques, we instead found that 4/5 cats did not survive the second round of anesthesia and surgery. In all of these cases the cats exhibited extreme tachypnea after a few minutes on moderate to low levels of isoflurane. Despite intervening with artificial ventilation, the breathing patterns did not recover after the withdrawal of anesthesia. Reanesthetizing and performing additional surgery on decerebrate cats is a somewhat common procedure and our negative outcomes seem to be

unique suggesting that some aspect of our initial surgery or robotic manipulation is the source of these complications. The 1 cat that survived the second surgery did not exhibit any head pitch dependent changes in either limb stiffness or to intermuscular reflex gains. While this single finding does not directly support our hypothesis, the lack of response to head tilt with both modalities in an otherwise normally responsive cat suggests experimental error is the cause.

4.4 Discussion

While the robotic measurements of hindlimb stiffness were not absolutely consistent, there was a distinct trend of reduced stiffness in the downslope condition which partially confirms our hypothesis. These findings mirror the results of our intermuscular reflex experiments which showed increased inhibition in the downslope condition. Considered together, these results are aligned with our grand hypothesis that the alteration of force dependent intermuscular reflexes is the mechanism responsible for the changes needed to interact with sloped environments.

The stiffness measurement in the upslope condition did not show a distinct trend when compared to level which contradicts our original hypothesis that a continuous trend of increasing stiffness would be observed with increased simulated slope angle. While a continuous, linear relationship between neck angle and limb stiffness would have been the simplest model for this relationship, the fact that the overall leg stiffness arises from the activities of discrete muscles suggests that the original hypothesis may have been overly simplistic. However, given that both neck and support surface angles can vary continuously within the range that we studied, we should at least expect that the relationship between stiffness and angle to be monotonic. Yet, this expectation was not

confirmed by our data. Our hypothesis was based upon the assumption that a single neural strategy is employed by all cats to perform sloped task successfully, but this may have been a flawed premise. Our decerebrate cat model is highly constrained and a majority of the cats' weight were supported by our equipment making it difficult to subjectively evaluate if the cats had different preferred postures in the upslope condition. While there was no trend to in limb stiffness in the upslope condition, this partially echoes our intermuscular reflex findings which were also least consistent in the head down trials. This is an additional indication suggesting that multiple strategies may have been employed giving the appearance of inconsistent results.

The measurements made under passive conditions were determined to be the most reliable because the baseline force returned to the same level between each perturbation and experienced the lowest frequency of paw-off events. However, while these may have been ideal conditions from a measurement perspective it might have been suboptimal neurologically. In the absence of measurable forces or EMG we were not able to ascertain if the decerebrate cats were truly exhibiting the same baseline neural patterns.

An additional concern with the low background activity associated with the passive condition is that subtle alterations in reflex gains due to the head pitch may be below the resolution of our measurements. Similarly, it is possible that the circuits responsible for the alterations require a minimum threshold of force or activity to be met in order to activate. If the baseline activity in the passive condition were slightly below this threshold, this might account for some of the observations where the limb stiffness seemed to be insensitive to head pitch.

While our attempts to increase the level of background force using XER and cutaneous stimulation were unsuitable for the measurement of 3D stiffness, it is possible that a stepping decerebrate cat would address the shortcomings of the other techniques. By allowing the robots to follow the paws throughout the step cycle, we would be able to repeatedly apply perturbations at specific points during the step cycle which should provide a higher baseline force than the passive condition and at a more predictable level than with XER or cutaneous stimulation. Additionally, we would expect a dramatic reduction in the number of paw-off events as the hindlimbs would be moving in a predictable pattern.

As compared to the results from our muscle puller experiments, the robotic stiffness measurements were much more variable despite using much of the same surgical procedures for both experimental paradigms. The greatest difference in the surgical preparation is the lack of muscular dissection in the shank which seems like it would reduce experimental variability rather than increase it. However, despite the more invasive surgery, the muscle puller experiments were considered successful when reflexes were measurable between a single pair of muscles. There were numerous cases where even the limited set of muscles measured were not all responsive throughout the experiment. If this unresponsiveness was due to variability in the brainstem transection rather than the muscle dissection, we would instead expect that measurements of the whole limb to be much more sensitive to differences in the decerebration and brainstem as differences in responsiveness in any hindlimb muscle would contribute to variability in the whole limb stiffness.

Despite our efforts to mitigate experimental variability the decerebrate cat model may simply have too many uncontrollable factors to allow reliable measurements using the robotic apparatus. Considering that we took care to minimize surgical disruption of the hindlimb to keep the leg as intact as possible, it should be possible to adapt these methods for use with trained cats or humans. Cats have previously been trained to perform ramp walking tasks (Maas et al. 2007) with chronically implanted EMG electrodes. Furthermore, since these experiments could be performed with minimal invasiveness, multiple series of measurements could be made with the same cat which could improve the statistical reliability of the stiffness measurements. The use of trained cats also does not preclude the performance of a terminal decerebrate experiment using traditional methods which could allow for comparisons of those results with those from this study. Human studies would employ surface EMG electrodes and while different techniques would need to be used to manipulate the body orientation signal, subject training and repeatability should be improved as compared to cats.

Although the experimental yield was low and we have identified some key aspects of the technique that can be improved, this study does provide some preliminary evidence that the body orientation signal signals the spinal cord to reduce hindlimb stiffness in the downslope condition which is consistent with our hypothesis based upon the biomechanical requirements for downslope walking.

CHAPTER 5

DISCUSSION

Overall, we found that the decerebrate cat had the strongest response to the body orientation signal in the downslope condition. This was manifested as increased force dependent inhibition between shank muscles as well as decreased stiffness in the entire hindlimb. While we did observe the opposite effect in the upslope conditions, these occurrences were not consistent enough to establish a definitive trend. It was the simplest hypothesis to assume that since the environment can be sloped at any arbitrary angle that the nervous system would likewise employ a single, continuously variable system to adjust to the slope condition. However, considering an idealized system, the transition between positive and negative slope angles corresponds to a shift in the need to expend energy for forward motion. While animals still need to expend energy to maintain controlled forward movements on a decline, the fact that much of the propulsive force is gravitational rather than muscular could represent a fundamental difference between downslope tasks compared to activities on a level or uphill surface. Based on this assumption, we would expect that the level and upslope patterns to be much more similar to each other than the downslope condition—a relationship which reflects our findings in both aspects of this study.

Another trend that we have revealed is that the increased intermuscular inhibition and correspondingly reduced limb stiffness associated with the downslope conditions seems to be present across numerous background motor patterns. Considering that standing, walking, and withdrawing from stimuli have very different behavioral functions the conservation of this effect suggests that the body orientation signal causing global

alterations which are passed through to all behavioral tasks. This manner of organization would serve to reduce the complexity of the neural circuitry needed to adapt to various sloped surfaces. Additionally, this would facilitate the transition between different behaviors as the changes due to the body orientation signal would persist between task transitions. As switching tasks is nearly as fundamental as the tasks themselves it stands to reason that an efficient system like this would be conserved amongst most vertebrate species.

Between both experimental modalities in this study, the results in the upslope conditions were somewhat inconsistent. While we expected that the uphill responses to the body orientation signal to produce a unified strategy as was the case with the downhill results, it is possible that there are multiple effective strategies that can result in successful uphill tasks. For example, if lowering the center of mass is the desired effect, it could be achieved either by widening the stance or decreasing total leg length. As we are measuring a small subset of leg muscles and experimentally constrain the leg position, we might not have enough information to discern if different strategies were employed by different cats. As previously discussed, it is technically feasible to adapt our experimental techniques for use with awake, trained cats. With these experiments it could be possible to determine if indeed different strategies are preferred by different cats and with a large sample, if the strategies cluster into distinct groups. Alternatively, as bipedal animals have a much smaller support area compared to overall body length, fewer strategies may be available and a better consensus could be found using human subjects.

While the head tilt with labyrinthectomy technique was developed prior to this study, it is not yet in widespread use. Our findings help to confirm that non-transient

alterations to the motor patterns can be attained using this method. We also discovered through the course of this study that the angular speed of neck rotation has a substantial influence on the longevity of the decerebrate cat preparation. One limitation of our process is that we do not currently have the ability to independently confirm the completeness of the labyrinthectomy. With the proper equipment it should be possible to use intercellular recordings to verify the abolishment of the vestibular signal in the decerebrate cat. Alternatively, the vestibular hair cells can be destroyed chemically using aminoglycosides like gentamicin. As this can be administered non-surgically, the elimination of a vestibular response can be verified behaviorally prior to the experiment. This method requires specialized veterinary care but eliminates the need for the labyrinthectomy surgery. This should also increase the experimental yield as it will eliminate the chance for an incomplete labyrinthectomy to give unreliable results.

The results of this study underscore the complexity of the interactions between various sensory systems. Efforts to rehabilitate and restore function after injury need to not only consider the lack of control that can result from sensory deficits, but also the possibility of partially remaining pathways providing improper modulation of motor activities. With a fuller understanding and mapping of the influence of the body orientation signal, new therapies could be developed to harness these pathways to improve task performance in changing environmental conditions. As our results seem to suggest that the body orientation signal has similar effects on different motor activities our techniques may have diagnostic relevance as to severity of injury since the effects should be visible with reflexive activities which may be unaffected by high spinal cord or brain injury.

We were also able to create a customizable robotic platform capable of making complex biomechanical measurements. By using commercially available components we have designed a system that can be easily replicated and used for other scientific endeavors. While the decerebrate cat did reveal some weaknesses in maintaining a reliable interface between the subject and the robots, this can be considered a near worst-case as their movements were strong and uncontrollable. In spite of this, we were able to increase our understanding of the physiological changes that allow for successful interactions with sloped support surfaces in addition to providing a platform for future investigations.

Due to the modularity and configurability of the robotic system this technology can be easily translated into use as a clinical diagnostic tool. As the workspace of the robotic arm encompasses the range of motion of human limbs our system can be programmed to make measurements on any limb or individual joints. The ability to use this system for a wide range of patients also offers the possibility of reducing overall capital costs by consolidating specialized equipment into a single device. Furthermore, making direct biomechanical measurements should improve reliability and repeatability of functional assessments by reducing evaluator variability.

REFERENCES

- Banks, R. W., M. Hulliger, et al. (2009). "A comparative analysis of the encapsulated end-organs of mammalian skeletal muscles and of their sensory nerve endings." J Anat **214**(6): 859-887.
- Bonasera, S. J. and T. R. Nichols (1994). "Mechanical actions of heterogenic reflexes linking long toe flexors with ankle and knee extensors of the cat hindlimb." J Neurophysiol **71**(3): 1096-1110.
- Boyle, R. and O. Pompeiano (1981). "Convergence and interaction of neck and macular vestibular inputs on vestibulospinal neurons." J Neurophysiol **45**(5): 852-868.
- Carlson-Kuhta, P., T. V. Trank, et al. (1998). "Forms of forward quadrupedal locomotion. II. A comparison of posture, hindlimb kinematics, and motor patterns for upslope and level walking." J Neurophysiol **79**(4): 1687-1701.
- Crouch, J. E. (1969). Text-Atlas of Cat Anatomy, Lea & Febiger.
- Eccles, J. C., R. M. Eccles, et al. (1957). "The convergence of monosynaptic excitatory afferents on to many different species of alpha motoneurons." J Physiol **137**(1): 22-50.
- Eccles, J. C., R. M. Eccles, et al. (1957). "Synaptic actions on motoneurons caused by impulses in Golgi tendon organ afferents." J Physiol **138**(2): 227-252.
- Ezure, K. and V. J. Wilson (1984). "Interaction of tonic neck and vestibular reflexes in the forelimb of the decerebrate cat." Exp Brain Res **54**(2): 289-292.
- Goslow, G. E., Jr., R. M. Reinking, et al. (1973). "The cat step cycle: hind limb joint angles and muscle lengths during unrestrained locomotion." J Morphol **141**(1): 1-41.
- Gottschall, J. S. and T. R. Nichols (2007). "Head pitch affects muscle activity in the decerebrate cat hindlimb during walking." Exp Brain Res **182**(1): 131-135.
- Gottschall, J. S. and T. R. Nichols (2011). "Neuromuscular strategies for the transitions between level and hill surfaces during walking." Philos Trans R Soc Lond B Biol Sci **366**(1570): 1565-1579.
- Green, P. R. (1998). "Head orientation and trajectory of locomotion during jumping and walking in domestic chicks." Brain Behav Evol **51**(1): 48-58.

- Gregor, R. J., D. W. Smith, et al. (2006). "Mechanics of slope walking in the cat: quantification of muscle load, length change, and ankle extensor EMG patterns." J Neurophysiol **95**(3): 1397-1409.
- Honeycutt, C. (2009). Mechanisms underlying muscle recruitment in response to postural perturbations. Ph.D., Georgia Institute of Technology.
- Honeycutt, C. F., J. S. Gottschall, et al. (2009). "Electromyographic responses from the hindlimb muscles of the decerebrate cat to horizontal support surface perturbations." J Neurophysiol **101**(6): 2751-2761.
- Honeycutt, C. F. and T. R. Nichols (2010). "The decerebrate cat generates the essential features of the force constraint strategy." J Neurophysiol **103**(6): 3266-3273.
- Houk, J. and E. Henneman (1967). "Responses of Golgi tendon organs to active contractions of the soleus muscle of the cat." J Neurophysiol **30**(3): 466-481.
- Hyingstrom, A., M. Johnson, et al. (2008). "Movement-related receptive fields of spinal motoneurons with active dendrites." J Physiol **586**(6): 1581-1593.
- Kandel, E. R., T. M. Jessell, et al. (2013). Principles of Neural Science, Fifth Edition, McGraw-Hill Education.
- Lawrence, J. H. and T. R. Nichols (1999). "A Three-Dimensional Biomechanical Analysis of the Cat Ankle Joint Complex: I. Active and Passive Postural Mechanics." Journal of Applied Biomechanics **15**(2): 95-105.
- Lawrence, J. H. and T. R. Nichols (1999). "A Three-Dimensional Biomechanical Analysis of the Cat Ankle Joint Complex: II. Effects of Ankle Joint Orientation on Evoked Isometric Joint Torque." Journal of Applied Biomechanics **15**(2): 106-119.
- Lyle, M. A. and T. R. Nichols (2018). "Patterns of intermuscular inhibitory force feedback across cat hindlimbs suggest a flexible system for regulating whole limb mechanics." J Neurophysiol **119**(2): 668-678.
- Maas, H., R. J. Gregor, et al. (2010). "Locomotor changes in length and EMG activity of feline medial gastrocnemius muscle following paralysis of two synergists." Exp Brain Res **203**(4): 681-692.
- Maas, H., B. I. Prilutsky, et al. (2007). "The effects of self-reinnervation of cat medial and lateral gastrocnemius muscles on hindlimb kinematics in slope walking." Exp Brain Res **181**(2): 377-393.
- Macpherson, J. M. (1988). "Strategies that simplify the control of quadrupedal stance. I. Forces at the ground." J Neurophysiol **60**(1): 204-217.

- Macpherson, J. M., D. S. Rushmer, et al. (1986). "Postural responses in the cat to unexpected rotations of the supporting surface: evidence for a centrally generated synergic organization." Exp Brain Res **62**(1): 152-160.
- Magnus, R. and A. de Kleijn (1912). "Die Abhängigkeit des Tonus der Extremitätenmuskeln von der Kopfstellung." Pflüger's Archiv für die gesamte Physiologie des Menschen und der Tiere **145**(10): 455-548.
- Martin, R. S. (2013). Implementation and validation of a computational model of the feline forelimb, Georgia Institute of Technology.
- Matthews, P. B. C. (1972). Mammalian muscle receptors and their central actions, Edward Arnold.
- McPhedran, A. M., R. B. Wuerker, et al. (1965). "Properties of Motor Units in a Homogeneous Red Muscle (Soleus) of the Cat." J Neurophysiol **28**: 71-84.
- Mori, S. and J. M. Brookhart (1968). "Characteristics of the postural reactions of the dog to a controlled disturbance." Am J Physiol **215**(2): 339-348.
- Mussa-Ivaldi, F. A., N. Hogan, et al. (1985). "Neural, mechanical, and geometric factors subserving arm posture in humans." J Neurosci **5**(10): 2732-2743.
- Nichols, T. R. (1989). "The organization of heterogenic reflexes among muscles crossing the ankle joint in the decerebrate cat." J Physiol **410**: 463-477.
- Nichols, T. R. (1999). "Receptor mechanisms underlying heterogenic reflexes among the triceps surae muscles of the cat." J Neurophysiol **81**(2): 467-478.
- Nichols, T. R. (2018). "Distributed force feedback in the spinal cord and the regulation of limb mechanics." J Neurophysiol **119**(3): 1186-1200.
- Nichols, T. R., T. C. Cope, et al. (1999). "Rapid spinal mechanisms of motor coordination." Exerc Sport Sci Rev **27**: 255-284.
- Nichols, T. R. and J. C. Houk (1976). "Improvement in linearity and regulation of stiffness that results from actions of stretch reflex." J Neurophysiol **39**(1): 119-142.
- Perreault, E., C. Heckman, et al. (2002). Three-dimensional moment and stiffness summation for muscles sharing a common tendon. Engineering in Medicine and Biology, 2002. 24th Annual Conference and the Annual Fall Meeting of the Biomedical Engineering Society EMBS/BMES Conference, 2002. Proceedings of the Second Joint, IEEE.

- Pierrot-Deseilligny, E. and D. Burke (2012). The Circuitry of the Human Spinal Cord: Spinal and Corticospinal Mechanisms of Movement, Cambridge University Press.
- Prilutsky, B. I. and V. M. Zatsiorsky (1994). "Tendon action of two-joint muscles: transfer of mechanical energy between joints during jumping, landing, and running." J Biomech **27**(1): 25-34.
- Putkonen, P. T., J. H. Courjon, et al. (1977). "Compensation of postural effects of hemilabyrinthectomy in the cat. A sensory substitution process?" Exp Brain Res **28**(3-4): 249-257.
- Ross, K. T. (2006). Quantitative Analysis of Feedback During Locomotion. Ph. D., Georgia Institute of Technology.
- Stahl, V. A. (2010). A biomechanical analysis of the role of the crural fascia in the cat hindlimb.
- Stahl, V. A. and T. R. Nichols (2011). "Short-term effects of muscular denervation and fasciotomy on global limb variables during locomotion in the decerebrate cat." Cells Tissues Organs **193**(5): 325-335.
- Stahl, V. A. and T. R. Nichols (2014). "Short-term effect of crural fasciotomy on kinematic variability and propulsion during level locomotion." J Mot Behav **46**(5): 339-349.
- van Eyken, A., S. Perlin, et al. (1987). "Robotic force platform for the study of posture and stance in the quadruped." Med Biol Eng Comput **25**(6): 693-697.